Quaternary Science Reviews 233 (2020) 106171

Contents lists available at ScienceDirect

Quaternary Science Reviews

journal homepage: www.elsevier.com/locate/quascirev

Coseismic coastal subsidence associated with unusually wide rupture of prehistoric earthquakes on the Kamchatka subduction zone: A record in buried erosional scarps and tsunami deposits

Pinegina T.K.[a], Bourgeois J.[b, *], Bazanova L.I.[a], Zelenin E.A.[c], Krasheninnikov S.P.[d], Portnyagin M.V.[e, d]

[a] Institute of Volcanology & Seismology FEB RAS, Petropavlovsk-Kamchatsky, Piip Boulevard 9, 683006, Russia
[b] Department of Earth and Space Sciences, University of Washington, 4000 15th Ave NE, Seattle, WA, 98195-1310, USA
[c] Geological Institute, Pyzhevsky Lane 7, Moscow, 119017, Russia
[d] V.I. Vernadsky Institute of Geochemistry and Analytical Chemistry, Kosygin St. 19, Moscow, 119991, Russia
[e] GEOMAR Helmholtz Center for Ocean Research Kiel, Wischhofstrasse 1-3, 24148, Kiel, Germany

ARTICLE INFO

Article history:
Received 30 October 2019
Received in revised form
10 January 2020
Accepted 13 January 2020
Available online xxx

Keywords:
Holocene
Paleoseismology
Kamchatka subduction zone
Geomorphology
Coastal
Ground penetrating radar
Tephrochronology
Coseismic coastal subsidence
Buried erosional scarps
Tsunami deposits
Beach ridges

ABSTRACT

The prograding strand plain of Avachinsky Bay, Kamchatka, Russia, along the highly active Kamchatka subduction zone, exhibits geological evidence–buried erosional scarps–for coseismic subsidence only three times in the last four millennia, the last event about 1200 years ago. This same coast has a historical record (since A.D. 1737) of five subduction-zone earthquakes with large tsunami runup (>5 m), the last of which was the 1952 Mw 9 Kamchatka earthquake, and a geological record of more than 30 large tsunamis in the last 4000 years. This rarity of buried scarps relative to large earthquakes contrasts with the Cascadia strand plain in SW Washington State, where most or all large events are represented by buried scarps. A strong factor in the amplitude and sign of coseismic deformation is distance from the seaward edge of a subduction zone (the trench); the Avachinsky Bay coastline is 180–200 km from the trench, with ~25° slab dip, requiring unusually wide ruptures to generate significant coseismic subsidence. This coastal zone is undergoing net subsidence approximately equivalent to the total of the three coseismic subsidence events, generating a sequence of beach ridges that increase in elevation seaward.

Each of the three unusual (coseismic subsidence) events comprises a) an earthquake whose deformation field caused b) onshore coseismic subsidence, thus local sea-level rise and c) sufficient deformation offshore to produce a large tsunami; a,b,c followed by d) a period of coastal erosion and shoreline retreat, leaving e) an erosional beach scarp that was f) subsequently buried once progradation resumed. We identified, dated and correlated the scarps and tsunami deposits from these events with several field methods, including trenching, tephrostratigraphy and ground penetrating radar. The scarps were correlated over an alongshore distance of 50–70 km. The most recent event (event 1) occurred ~800 cal AD (1100–1250 ^{14}C years BP), event 2–600 cal BC (2400–2450 ^{14}C years BP), and event 3–1700 cal BC (3300–3500 ^{14}C years BP). We developed methods for quantifying subsidence, coastal erosion and tsunami size for each of these events. All three retain evidence of ~0.4–1.2 m of coseismic subsidence; coastal erosion in the case of event 1 averaged more than 100 m; all three "event" tsunamis were amongst the largest in the last 4000 years.

1. Introduction

One of the most stratigraphically distinctive records of great subduction-zone earthquakes is the indication of onshore coseismic subsidence, typically as recorded by buried soils (Nelson et al., 1996), but also by buried (beach) scarps (Meyers et al., 1996), the latter a primary focus of this paper. Historical records with measurements of coseismic subsidence, as well as uplift, begin with surveys after Nankai Trough events in the 1940s, followed by Chile 1960 and Alaska 1964 earthquakes, with significant details added

* Corresponding author.
E-mail address: jbourgeo@uw.edu (J. Bourgeois).

https://doi.org/10.1016/j.quascirev.2020.106171
0277-3791/

from the Sumatra 2004, Chile 2010 and Tohoku 2011 events. The A.D. 1700 Cascadia earthquake, while considered historical based on tsunami records in Japan, is best understood by its stratigraphic and paleontologic record of coastal deformation from British Columbia to northern California (summarized in Leonard et al., 2004; Wang et al., 2013). The amount of coseismic land-level change in any one event is determined by several factors, including width of the rupture, distance from the subduction zone and amount of slip (e.g., Leonard et al., 2010). The length and along-strike position of the rupture are also factors (e.g., Dura et al., 2017), as can be elastic heterogeneity (Hashima et al., 2016).

The distance from the Kamchatka coast to the axis of the Kuril-Kamchatka trench–the seaward edge of the subduction zone–varies from about 80 to 200 km (Fig. 1), which has an important impact on onshore coseismic crustal deformation (Fig. 2). Using the method of Okada (1985), Pinegina (2014) showed that only the strongest subduction-type earthquakes with a source width on the order of 150 km or more can cause noticeable coseismic subsidence on the broadly recessive parts of the Kamchatka coast such as Avachinsky Bay (Fig. 2). Such a result was also shown by Satake et al. (2008) for Hokkaido, at the southern end of the Kuril-Kamchatka trench; they concluded, in the same analysis, that the widest earthquakes did not necessarily produce the largest tsunami runup/inundation. In the case of Kamchatka's Avachinsky Bay, the subject of this study, the widest ruptures are recorded by buried scarps as well as by tsunami deposits. Notably, at Avachinsky Bay, marker tephra are abundant enough that ages can be assigned to these scarps, and specific tsunami deposits can be correlated with them (Pinegina et al., 2018). Thus, we can investigate a relationship between these wide earthquakes and the size of their tsunamis. At the same time, essentially as an unintended outcome, we also address the relationship between coseismic subsidence and beach ridges along subduction-zone coastlines.

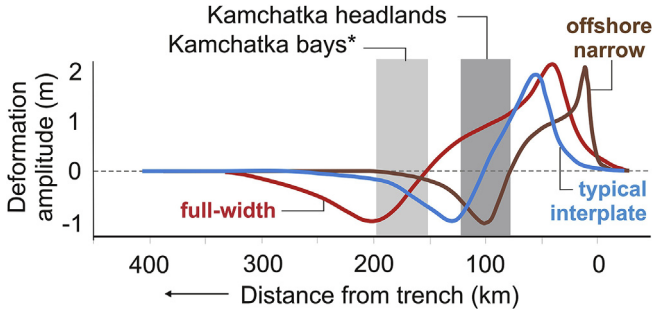

Fig. 2. An example model of coseismic deformation in Kamchatka (Pinegina, 2014), using Okada (1985); also see Satake et al. (2008) for Hokkaido example. *Kamchatka bays include Avachinsky, the subject of this study.

1.1. Subduction-zone earthquake deformation

A typical subduction-zone rupture produces trenchward uplift and landward subsidence (e.g., Thatcher and Rundle, 1979) (Fig. 2). This motion occurs not only offshore, where the deformation generates tsunamis, but also onshore, typically in the coastal zone, including offshore islands such as Isla Mocha, Chile (Melnick et al.,

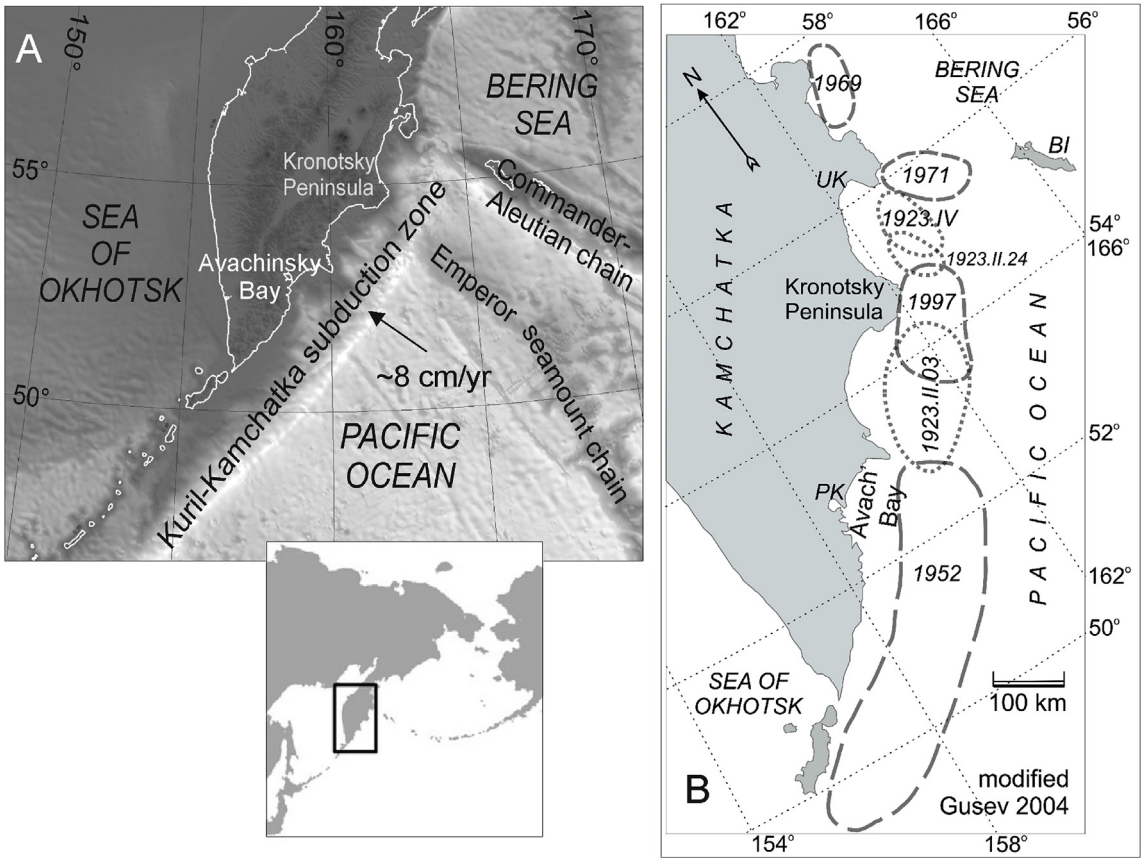

Fig. 1. Location of the Kuril-Kamchatka subduction zone (A), with outlines of 20th century large and great earthquakes (B, modified after Gusev, 2004). Heavier dashed lines are better located earthquake sources. "Avach Bay" - Avachinsky Bay. PK – Petropavlovsk- Kamchatsky, UK – Ust' Kamchatsk, BI – Bering Island. 1923 earthquakes are identified by month (Roman numerals) and day; e.g., 1923.II.24 is February 24, 1923.

2006); Kodiak, Alaska (Plafker, 1965, 1969); Simeulue and Nias, Indonesia (Meltzner et al., 2006). Deformation may take place almost entirely offshore if the rupture width is narrow, or if the continental shelf is wide, where the coastline is on the order of 200 km from the trench, as in Hokkaido (Satake et al., 2008), (western) mainland Aceh (Meltzner et al., 2006) and (eastern) northern Honshu (Imakiire and Koarai, 2012).

Until very recently, only near-coastal coseismic deformation had been historically quantified, using tide gages and other markers of sea level. Examples of systematic documentation of coseismic deformation from 20th century subduction-zone earthquakes include the Nankai trough in Japan (1944 & 1946 events, summarized in Ando, 1975) and the two mega-earthquakes of the 1960s – Mw 9.5 Chile 1960 (Plafker and Savage, 1970; Barrientos and Ward, 1990) and Mw 9.2 Alaska 1964 (Plafker, 1969). From these and 21st century examples amplitudes of historical subduction-zone coseismic deformation registered in coastal areas has reached up to +2 to +5 m (max +5.7 excluding splay faulting) uplift, and −0.5 to −2 m (max −2.7) subsidence. In general, documented and modeled (Fig. 2) uplift seaward of subsidence is about 2x the subsidence for any given case (e.g., Plafker, 1965 for Alaska 1964; Plafker and Savage, 1970 for Chile 1960; Meltzner et al., 2006 for Sumatra 2004; Melnick et al., 2012, Farías et al., 2010 for Chile 2010; Gusman et al., 2012 for Tohoku 2011).

Coseismic deformation is controlled by several factors; deformation is not tied to location of the shoreline, but rather to distance from the trench and the type of rupture (Fig. 2). In the modeled example in Fig. 2, rupture width is the primary factor. Other factors include fault dip angle and slip amount, as well as position of the rupture along strike (Okada, 1985).

1.2. Reconstructing subduction-zone earthquakes

Quantifying the parameters of subduction-zone earthquakes–their magnitude, and particularly their deformation field–can use several different techniques. In the pre-instrumental historic period, one could use shaking intensity based on eyewitness accounts (as in Gusev and Shumilina, 2000). For the instrumental period, most commonly used are seismic records (e.g., Lay et al., 2009, for Kurils 2006, 2007 earthquakes) and more recently, geodetic deformation (e.g., Bürgmann et al., 2001, for 1997 Kronotsky earthquake; GSI website for Tohoku earthquake (http://www.gsi.go.jp/cais/topic110421-index- e.html; see also Kobayashi et al., 2011; Imakiire and Koarai, 2012). Because coseismic deformation under water generates a tsunami, another means for reconstructing this deformation is to invert far-field tide-gage records (e.g., Johnson and Satake, 1999) or near-field runup distribution of a tsunami (e.g., MacInnes et al., 2010), both for Kamchatka 1952 earthquake; see Satake (2015) for a review of events in Japan.

Along affected coastlines, as noted above, tide-gage records of abrupt sea-level change are commonly used to quantify coseismic deformation, though many coastlines have few such gages, and large-amplitude deformation may remove a tide gage from its useful range. Only very recently, GPS and other satellite-based measurements have become accurate enough in the vertical range. Thus historically and even recently, the displacement of attached benthic coastal organisms such as corals (Sieh et al., 2008) and mussels (Melnick et al., 2012) has been a major way to quantify and map coseismic uplift, and, with more difficulty, subsidence ("drowning" of these organisms). The most common method for quantifying prehistoric vertical changes also uses sensitive sea- and tide-level indicators such as coastal vegetation, mollusks and microbenthos (e.g., Shennan and Hamilton, 2006; Arcos, 2012; Pilarczyk et al., 2014; Dura et al., 2016), particularly in cases where there are coastal wetlands.

It remains a challenge to document and quantify coseismic deformation along high-energy, open-coast, sandy settings (beach-ridge or strand plains) such as parts of Cascadia and much of Kamchatka and the Kuril Islands, where the only record of coseismic deformation may be changes in topography related to sea level, buried erosional scarps, and associated tsunamis. In this study we address cases of co-seismic subsidence and tsunami genesis along the eastern Kamchatka coastline, in particular along Avachinsky Bay (Figs. 1 and 3), with examples from other embayments. We show that along this bay only three of more than 30 tsunamigenic events in the last 4000 years can be directly tied to evidence of

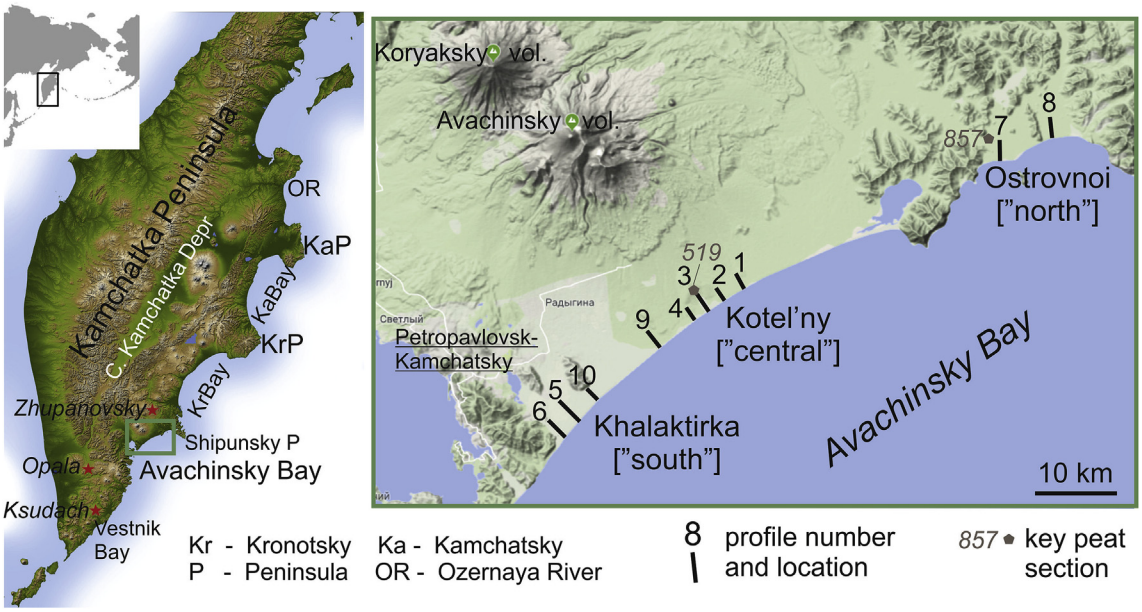

Fig. 3. Location of field sites used in this study, with a focus on Avachinsky Bay profiles. More background on the Avachinsky Bay site, including details on historical seismicity, geomorphology and sea-level trends is presented in Pinegina et al. (2018).

substantial coseismic subsidence, the latter as evidenced by buried beach scarps that record coastal retreat following abrupt sea-level rise. In doing so, we review the nature of buried beach scarps associated with coseismic subsidence and illustrate methods for identifying and quantifying the record of these buried scarps. Beach ridges and their heights are of secondary importance in this study–their origins and heights are various and complex (Tamura, 2012); we will argue, in any case, that they are not reliable paleoseismic indicators (section 5.3).

1.3. Buried beach scarps as coseismic indicators—concepts and methods

A "buried scarp" in our usage (also Meyers et al., 1996) is an erosional beach scarp that has been subsequently abandoned and buried, typically by a subsequent phase of coastal deposition, leading to progradation—a seaward advance of the shoreline. Erosional beach scarps are common on sandy shorelines, generated most often by temporal increases in wave energy such as erosion during storms, but also by processes such as river-mouth migration (review by Tamura, 2012). Sea-level rise, whether transient during a storm surge or long-term as generated by change in global ice volume, has been shown to result in erosion and coastline retreat, as quantified, e.g., by Bruun's rule (Bruun, 1962; Peterson et al., 2000). Shorter-term (e.g., El Niño) or longer-term (e.g., Little Ice Age) variations in wave climate and sea level can generate alternating periods of erosion and deposition, leaving erosional scarps buried by subsequent progradation (e.g., Buynevich et al., 2007). Coastal co-seismic subsidence is a special case of abrupt local to regional sea-level rise, to be expected along active fault zones.

In a pioneering paper, Meyers et al. (1996) identified a sequence of eight buried scarps along the SW coast of Washington State, part of the Cascadia subduction zone, and associated them with prehistoric incidences of coseismic subsidence spanning almost 6000 years. Their primary methods involved subsurface profiling with Ground Penetrating Radar (GPR) as well as vibracoring to understand the nature of radar reflections associated with the scarps. With AMS radiocarbon dating, they correlated several scarps to previously identified and dated evidence for subduction-zone earthquakes. This work was expanded geographically and updated chronologically by Peterson et al. (2010). To our knowledge, none of these scarps has been excavated.

Recently, a similar series of at least 7 buried scarps has been identified in Chile midway along the rupture zone of the Mw 9.5 1960 earthquake (Cisternas et al., 2017), which resulted in widespread coastal subsidence (Plafker and Savage, 1970). These scarps have been located by GPR, studied in excavation, and compared to the historical 1960 case; in some cases they have a capping shore-parallel ridge (Cisternas et al., 2017; M. Cisternas, personal communication).

1.4. Generating a buried coseismic scarp

The process of generating a buried scarp associated with a subduction-zone earthquake is as follows (Fig. 4; also see Meyers et al., 1996; Peterson et al., 2010). After coseismic subsidence, the abrupt rise in relative sea level will induce landward erosion, as shown in actual historical cases in Chile (Cisternas et al., 2017), Alaska (e.g., Saltonstall and Carver, 2003; Crowell and Mann, 1996) and Indonesia (Monecke et al., 2015). This erosion commonly produces a scarp, and the new, active beach will come in contact with an older part of the preserved wave-built terrace, which in Kamchatka cases is typically a "soil-pyroclastic sequence" (SPS) — an accumulation of soil or peat interbedded with tephra layers (and

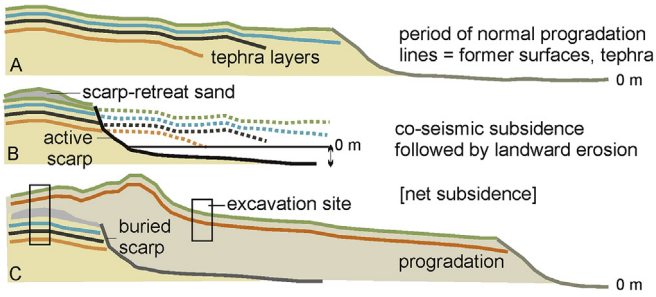

Fig. 4. Cartoon of a prograding shoreline (A) interrupted by coseismic subsidence (B), and then resumed progradation (C). In (C), excavations on either side of the scarp contain different tephra sequences. Cartoon based on outcrop in Vestnik Bay (Fig. 3), exposed in long river cutbank (more detail in Electronic supplement Fig. A2).

potentially with tsunami or storm deposits) (Fig. 5). During erosional retreat, storm sands pile up just landward of the scarp; we call this the "scarp retreat sand" (SRS) (Figs. 4 and 5). After some time, a new sediment-equilibrium profile will be established along the shore, and if the sediment supply is positive a progradational stage will recommence (Fig. 4). The contact line between the older terrace and the younger (post-seismic) terrace is a buried scarp.

1.5. Distinguishing a coseismic-subsidence-induced buried scarp from other scarps

Criteria for identifying coseismic-associated scarps include continuity in age for some distance along the coast (e.g., Peterson et al., 2010); coincidence in age with tsunami deposits or with a rise in wave-built terrace elevation; and correlation with the age of an abrupt boundary of peat or soil overlain by muddy sediments (e.g., tide-flat or lagoonal sediments) (a "buried soil"; e.g., Nelson et al., 1996). These scarps are characterized by a scarp-retreat sand overlying a soil profile, into which erosion produces a steep, undercut upper face that commonly fails, generating soil-block colluvium (e.g., Fig. 5). Heavy minerals are commonly concentrated on the lower, less steep portion of the scarp (e.g., Meyers et al., 1996).

There has been some discussion as to whether coseismic examples of buried scarps or scours represent primarily short-term tsunami erosion (hours) vs. longer-term coastal retreat (years)

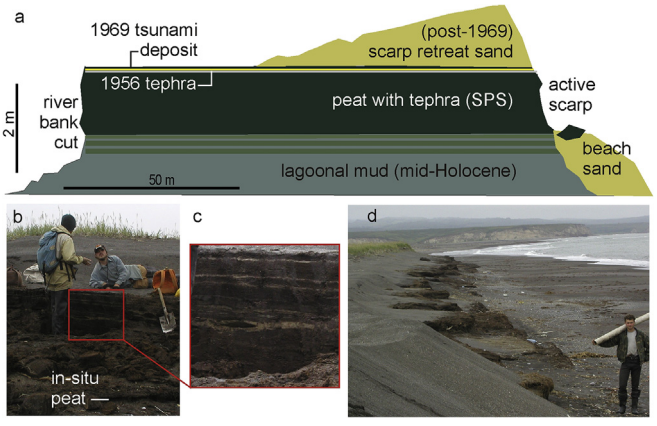

Fig. 5. Example of an actively eroding beach scarp, near Ozernaya River mouth (Fig. 3); a - measured profile with internal stratigraphy confirmed by outcrop on seaward and landward sides, V.E. ~15; SPS = soil-pyroclastic sequence. b-d - photos of the scarp and scarp excavation; lowest tephra in the peat (c) is ~4000 years old. It is possible that scarp erosion was initiated or enhanced by coseismic subsidence in 1969 (see Martin et al., 2008).

Fig. 6. The position of a buried scarp (dashed line on the photo) in this case coincides with the change of forest vegetation to grass; the scarp is probably from 1737 Kamchatka earthquake (the sand overlapping the scarp includes KSht$_3$ tephra 1907 AD). Photo from Sarannaya Bay south of Petropavlovsk-Kamchatsky by E.A. Kravchunovskaya.

(e.g., Simms et al., 2017). While recent tsunamis have caused substantial erosion, the erosional surfaces are typically diverse, irregular surfaces such as breaches in ridges and channels from return flow (e.g., MacInnes et al., 2009; Morton et al., 2011; Richmond et al., 2012; Udo et al., 2012). Simms et al. (2017) use irregularity in a GPR-identified, buried scour to contrast that paleo-scour with the smooth, concave-up scours (in GPR records) described by Meyers et al. (1996). Only deep tsunami scours will be distinct as geological traces, and there will not be a scarp retreat sand (Figs. 4 and 5), nor should there be distinct concentrations of heavy minerals.

Compared to storm-generated scarps (e.g. Buynevich et al., 2007), coseismic scarps will have lower recurrence intervals and will tend to erode more deeply into old soil profiles. Most storm scarps will have short life spans, but some will be preserved (e.g., Buynevich et al., 2007) and may superficially resemble coseismic scarps. As noted above, the coseismic cases should be associated with other indicators of the earthquake, such as tsunami deposits, a change in (wave-built) terrace elevation, or correlative buried marsh soils or drowned forests.

1.6. Locating and dating buried scarps

In order to locate buried scarps prior to field studies, analysis of aerial photographs and satellite images may help because different-aged soils will host different vegetation communities (e.g., Kravchunovskaya et al., 2010) (Fig. 6). Another method for buried-scarp location is the profiling of accumulative terraces with Ground Penetrating Radar (GPR) (e.g., Meyers et al., 1996; Peterson et al., 2010). Scarps may be associated with ridges, because of the overlying scarp-retreat sand (Figs. 4 and 5), but this is not always the case (e.g., Meyers et al., 1996; this paper). The exact location of a buried scarp may require continuous or closely spaced excavations; ground penetrating radar (GPR) (Fig. 7) can be used to choose a site to trench.

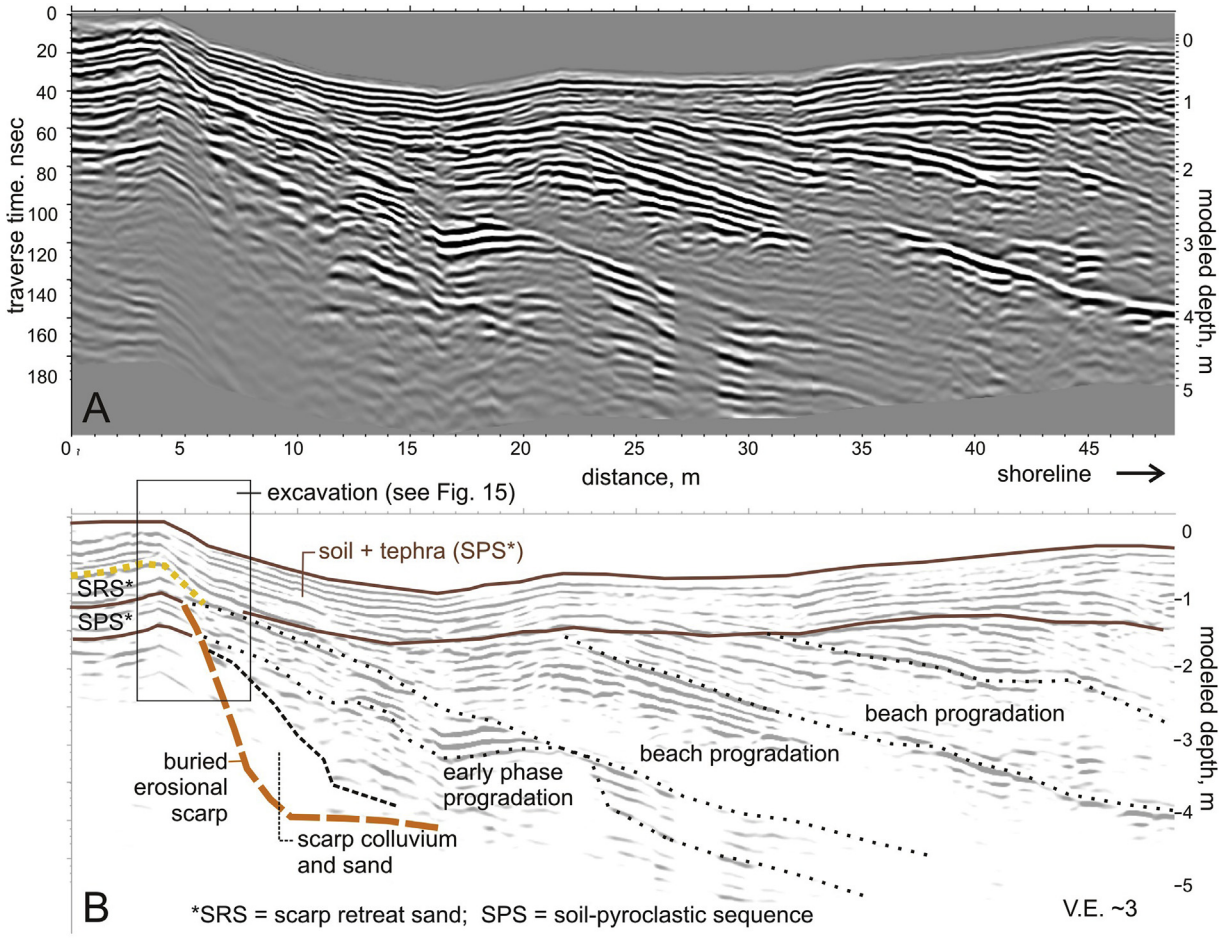

Fig. 7. Example of GPR profile across a buried erosional scarp. (A) and its interpretation (B). The shoreline is to the right.

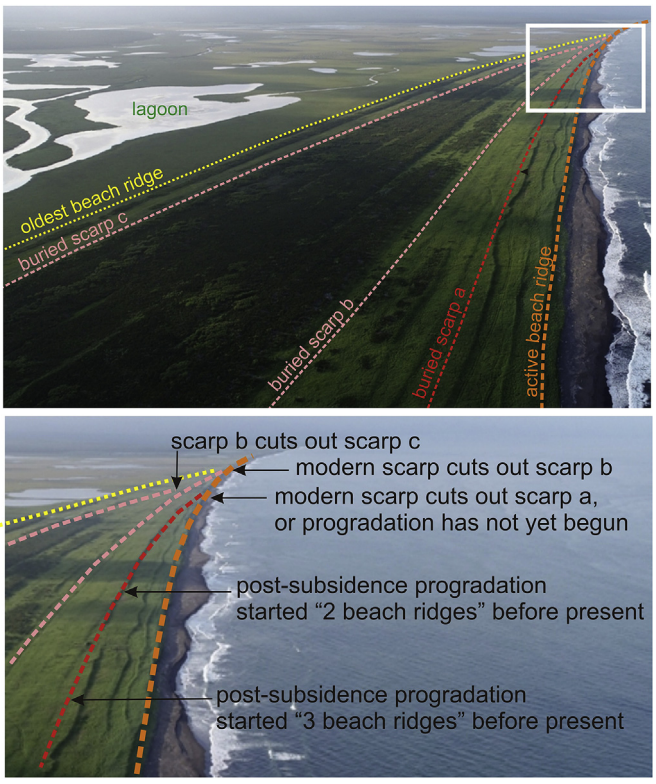

Fig. 8. Oblique air (drone) photo looking north along southern Kronotsky Bay (Fig. 3), alongshore distance about 10 km. Buried scarps have been mapped via GPR and excavations, but the case can also be considered just based on relative ages. There is increased sediment supply toward the south, and/or increased erosion toward the north. Thus this case shows how the determined timing of coseismic subsidence (time between cessation of post-subsidence erosion and subsequent initiation of progradation) can vary in accuracy/time span along a shoreline. More rapid progradation generates more accurate ages for the coseismic subsidence that led to a (buried) scarp.

In the field, in order to find buried scarps, we look for cases where adjacent excavations along a profile have a significant difference in age of the soil-pyroclastic sequence (SPS), based on tephra (e.g., Fig. 4). The (limiting) age of a portion of the coastal plain can be determined by the lowermost tephra in a proximal excavation, which roughly corresponds to the time when the beach became inactive, as the coast prograded (e.g., Fig. 4). At this time of tephra deposition, soil overlying the area proximal to the beach became stable, and the SPS began to accumulate above beach and storm sands. Thus, if the SPS in two adjacent excavations is notably different in age, there will likely be a buried erosional scarp between them.

We can determine the age range during which coseismic subsidence occurred as between the (youngest) age the buried surface on the landward side of the scarp and the oldest age of the overlying/overlapping beach sediments. In order to generate such ages, we need datable material. In practice, age determination can be difficult because the amount of landward erosion may vary along the coast due to several factors, including variations in subsidence amplitude, in wave energy and in progradation rate (sediment supply). For the same reasons, the time of resumption of accumulation along the coast can differ. Kronotsky Bay (Fig. 8) shows such an example, where beach ridges are not parallel with each other but converge. Peterson et al. (2010) found that following subsidence-induced coastal retreat, there was a "delayed onset of shoreline progradation with increasing distance from the Columbia River mouth" (sediment source). In the case of Avachinsky Bay, the focus of this study, beach ridges remain shore-parallel, which simplifies scarp correlation.

The ability to identify and date buried scarps is enhanced by rapid progradation, overall (e.g., Fig. 8 to the south), and by abundant tephra closely spaced in time; both criteria are met in the Avachinsky Bay case study herein. The *net* progradation rate along Avachinsky Bay is quite high, averaging ~0.2 m/yr for the 10 profiles (details below), so that without erosional episodes, adjacent excavations have soil-pyroclastic sequences very close in age. Distinctive tephra layers have typical recurrence intervals of 100–300 years, less in profiles closer to Avachinsky volcano (Fig. 3), with somewhat longer intervals farther away. Scarp recurrence intervals in this case are on the order of 1000 years.

2. Methods

2.1. Profiles and excavations

During field investigations along about 70 km of Avachinsky Bay we measured 10 topographic profiles perpendicular to the coastline (Figs. 3 and 9) and described ~150 soil and peat sections. These profiles are grouped into three sites (Fig. 3): south (Khalaktirka), central (Kotel'ny) and north (Ostrovnoi) (Fig. 3); four of the profiles (central 1, 3; north 7, 8) have been studied in most detail and receive the most attention in this paper; the (southern) Khalaktirka profiles are more anthropogenically disturbed and haven't as many preserved beach ridges. We measured topographic profiles using a tripod, level and rod (vertical accuracy on scale of centimeters, horizontal on scale of decimeters), or with a Trimble M-3 total station (distance measurement accuracy of ±3 mm/km and angular accuracy of ±1″). The elevations of profiles 1, 3, 7, 8 and 9 are relative to the Point of the State Geodetic Network, and the other

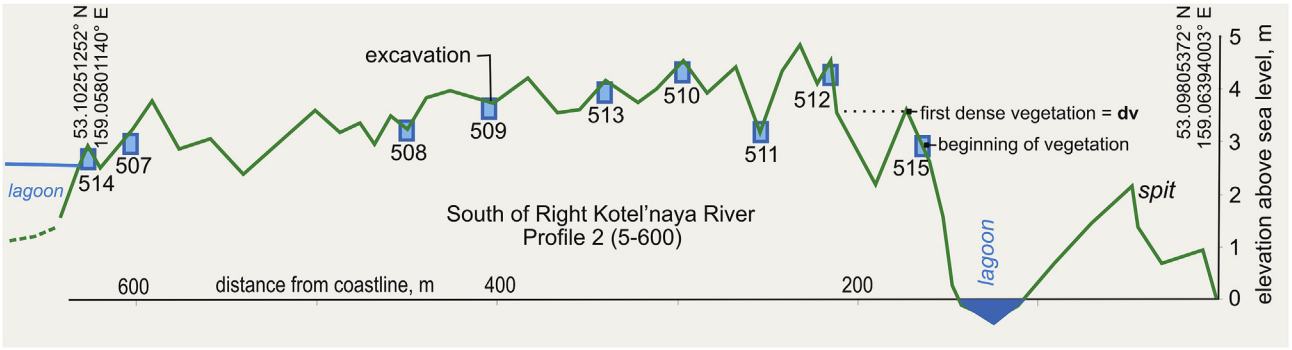

Fig. 9. Example (Profile 2, located on Fig. 3) of a topographic profile measured across the beach-ridge plain, showing locations of excavations. Vertical exaggeration ~30. Note elevation of first dense vegetation (**dv**), below 512, which is the lowest point on the shore profile where soil begins to form.

five are relative to sea level corrected for tide. On each profile we noted the elevation from the shore of the first beach vegetation and of the first dense vegetation (**dv**) (as in Fig. 9). We associate **dv** with the current lowest elevation, at the shoreline, at which soil forms, and thus correlative with the oldest paleosol above clean beach sand in any excavation (more details in Pinegina et al., 2013; Pinegina et al., 2018). We hand dug excavations through the soil-pyroclastic sequence down to clean beach/storm sand. In cases where a buried scarp was located and digging was possible, excavations were widened or lengthened to expose the scarp. In each excavation, we measured and described the geological section and identified, described, and in some cases sampled deposits of volcanic ash (tephra) and tsunami sand.

2.2. Tephra stratigraphy, analysis and chronology

Tephra studies with field description, radiocarbon dating, and chemical analysis provide comprehensive stratigraphic and chronological control for prehistoric events (e.g., Lowe, 2011; Ponomareva et al., 2017; Pinegina and Bourgeois, 2020). For stratigraphic markers along Avachinsky Bay we use well-known tephras from large Holocene eruptions on southern Kamchatka (Kyle et al., 2011; Braitseva et al., 1997a, b) as well as additional, more local tephra from Avachinsky volcano, and two tephra deposits from eruptive vents of Zhupanovsky volcano (ZH2050 - Main cone, PR2150 - Priemysh cone) (Pinegina et al., 2018, and this paper).

In the field, we described tephra layers by stratigraphic position and by appearance–thickness, grain size, grading, color of particles, lithic content, textural features, etc. Layers were then identified/indexed by tracking to and comparing with previously studied tephra in sections toward Avachinsky volcanic complex, as well as by stratigraphic position relative to regional marker tephra. Isopach maps and/or dispersal axes have been compiled for most Avachinsky fall units so the presence of a particular tephra at a given location can be predicted. We also sampled key tephra for chemical analysis/tracking and collected peat samples for radiocarbon dating.

Radiocarbon dates were produced at the Geological Institute of the Russian Academy of Sciences (Moscow) and at the Institute of Volcanology, Far-Eastern Branch of the Russian Academy of Sciences (Petropavlovsk-Kamchatsky). Avachinsky tephra are assigned names (e.g., "AV2650") based on averaged radiocarbon dates. Major elements of volcanic glass shards from proximal tephra samples of Avachinsky volcano and marker tephra were analyzed using the JEOL JXA 8200 electron microprobe at Geomar (Kiel, Germany) following procedure described in Ponomareva et al. (2017). The tephra database consists of 58 samples representing 43 Holocene eruptions of Avachinsky volcano identified using tephrostratigraphic investigation of soil-pyroclastic deposits around the Avachinsky group of volcanoes. Details of methods and results of radiocarbon dating are in Electronic Supplement Text A, Table A1; geochemical data are presented in Electronic Supplement Table B1.

2.3. Ground penetrating radar (GPR)

Ground penetrating radar (GPR) is used to generate a continuous record of near-surface stratification and discontinuities (Fig. 7) (Bristow and Jol, 2003). GPR can work well in coastal-plain sequences comprising layers differing in resistivity, such as a tephra layer in soil, or a heavy-mineral layer in sand. Usually, on radargrams measured through prograding strand plains, there are visible reflection signals corresponding to the boundaries of sand or pebble layers sloping toward the sea (Fig. 7). GPR profiles must be tied to topographic profiles for proper interpretation; for the study of shore progradation and buried scarps, these profiles are perpendicular to the shoreline and to beach-ridge strike. We used the Russian GPR "Oko" made by the firm "Logis," and a shielded aerial unit with a center frequency of 700, 250 and 50–100 MHz.

A buried scarp on a radargram is typically steeply dipping and thus does not generate its own reflection but is expressed by the termination of normal, prograding stratification (e.g., Fig. 7). Often, on the lower, more gently dipping part of this erosional-retreat boundary, there is an accumulation of heavy minerals, which amplifies the reflective signal on the radargram (e.g., Meyers et al., 1996). In this study, from radargrams, we located possible buried scarps, hand dug trenches to expose the scarps, and studied their structure and stratigraphy.

2.4. Quantifying subsidence and erosion

2.4.1. Subsidence

Without water-level-sensitive organisms, as discussed above (section 1.2), quantifying the amount of (prehistoric) coseismic subsidence on either side of a scarp is challenging. Essentially, an elevation marker/indicator relative to sea level is needed before and after subsidence. We cannot simply use topography directly on either side of a scarp because we cannot determine exactly which topographic part of a profile (e.g., trough or ridge) was preserved just landward of a scarp, and subsequent progradation also generates irregular topography. This topography is controlled not only by sea level, but also by wind erosion and deposition, and water erosion. Thus we use differences in *average* heights landward and seaward of a scarp, or differences in stratigraphic indicators of a reference height – the lowest elevation at which soil is established on a beach profile ("**dv**" on Fig. 9). The differences may involve decades to centuries, so the results do not account for interseismic vertical offset. This issue will be discussed after data and analysis.

We tried three different methods of quantifying coseismic subsidence in this study (Fig. 10). The first method (Method 1, "educated eye"), used by Pinegina (2014), is based on information both from profiles and from excavations to estimate coseismic subsidence, with a focus on beach ridge heights (Fig. 10). We subsequently developed a variation on this method by taking profile elevation data in a spreadsheet and calculating the average trend lines for topography on either side of a scarp (Method 2, "trend calculation") (Fig. 10). Thirdly (Method 3, "**dv** elevation difference"), we measured the elevation difference of the oldest soil landward and seaward of a buried scarp, either within the trench of an excavated scarp (Method 3a) or in excavations proximal to a located, but unexcavated, scarp (Method 3b) (Fig. 10). Method 3 interprets the base of the oldest soil to represent the elevation of first dense vegetation (**dv**, Fig. 9) on a beach profile when the beach resumed progradation.

None of these methods is precise, with error not easy to quantify; we tried all three and discuss results below. Because beach-ridge plain elevations are easily affected by processes not related to sea level, as noted above, we expect Methods 1 and 2 to be rough.; Method 2 might be better because it averages all elevations. Method 3 depends on recognizing and equating oldest soil in an excavation to a point related directly to sea level.

2.4.2. Erosion and progradation

We estimated the amount of horizontal erosion (post-subsidence coastal retreat, followed by resumed progradation) by examining shortened distances between dated scarps compared to predicted distances based on elapsed time multiplied by long-term net progradation rates. If quantified subsidence amounts are accurate, and the offshore profile is known, it is also possible to predict erosion using Bruun's rule, or to postdict subsidence based on quantified erosion. For example, using Bruun's rule for the

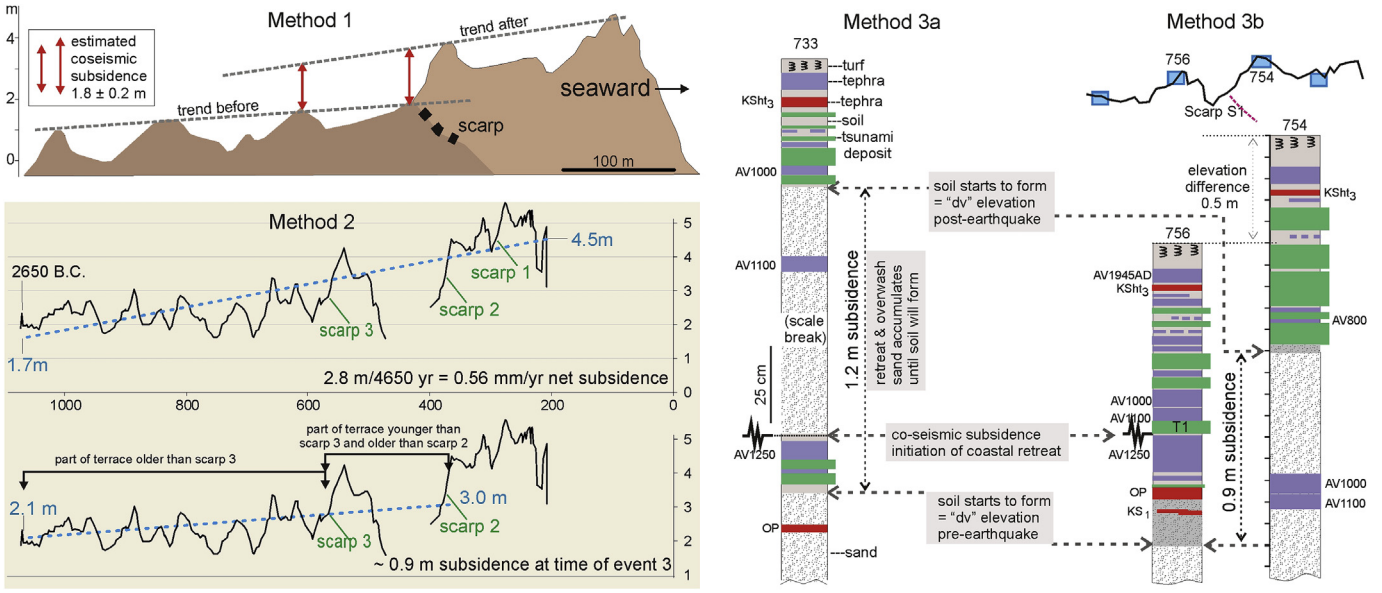

Fig. 10. Three means for making a quantitative estimate of prehistoric coseismic subsidence on a sandy strand plain, with actual examples from Kamchatka field sites; the basic process of generating a buried scarp is illustrated in Fig. 4. **Method 1** (profile example from south Kamchatsky Bay, Storozh site) – the "educated eye" method uses graphic plots of profiles to generate average beach ridge elevations landward and seaward of a scarp (as in Pinegina, 2014). **Method 2** (example extracted from central Avachinsky Bay profile 1) takes Excel-plotted parts of the profile and generates an average elevation trend, the difference between each end being an estimate of subsidence; this method is affected by particularly low zones such as current or former river channels; in this example, the low zone was not included. **Method 3** measures the difference in elevation of oldest soil before and oldest soil after a coseismic subsidence event, with this elevation representing the establishment of dense vegetation (**dv**, as in Fig. 9) on a beach profile as it progrades. Method 3a (example of Scarp S1 on profile 3, see details in results) can be applied when a trench exposes a buried scarp, using the section just landward of the scarp; Method 3b (example of Scarp S1 on profile 1) is used when the scarp is not (fully) exposed, with the choice of excavation landward and seaward approximating the same *relative* elevation (e.g., ridges on either side in this case); T1 – tsunami deposit from the same event with Scarp 1.

setting of sandy Cascadia shorelines, Peterson et al. (2000) modeled erosional retreat of ~30–60 m for 0.5 m subsidence; ~70–240 m for 1 m subsidence; and 260–300+ m for 1.5 m subsidence. Erosion amounts on the order of 100 m are consistent with documented historical cases from Alaska 1964 (Saltonstall and Carver, 2003; Crowell and Mann, 1996) and Aceh 2004 (Monecke et al., 2015). In Alaska, new sandy beaches had formed following retreat by the 1990s, probably earlier; in Aceh the shoreline was mostly "healed" within a few years. In Chile, post-1960 erosional retreat "turned around" to progradation by 1979 (Cisternas et al., 2017).

2.5. Quantifying tsunami size

In each excavation along a measured profile, we identified tsunami deposits and described their thickness, grain size, stratification and grading. Tsunami deposits in soil-pyroclastic sequences along Avachinsky Bay are generally thin sand layers (up to 20 cm thick), which tend to decrease landward in both thickness and grain size. The deposits consist mostly of the same material as the accumulating strand plain and active beach – mainly dark, medium-to coarse-grained sand with some layers and patches of rounded gravel and pebbles. More details of identification criteria are presented in Pinegina et al. (2018).

We determined a minimum distance (sediment inundation, L) and a minimum height (sediment runup at inundation point, H) of past historical and prehistoric tsunamis from tsunami-deposit distribution (Electronic Supplement Fig. A3). The most landward section with a given tsunami deposit approximates tsunami runup and inundation. If the tsunami crossed the beach-ridge plain orthogonally, the reconstructed tsunami height may also be bounded by the maximum elevation (h) of beach ridges between the shoreline and tsunami-deposit pinch-out (ES Fig. A3). For accurate estimation of paleotsunami runup and inundation, for each paleotsunami, we reconstructed the (paleo)shoreline position and (paleo)surface elevation at the time of tsunami deposition, using tephra stratigraphy and tephra mapping along measured topographic profiles (method details in Pinegina et al., 2018).

In this comparative study of multiple profiles in the same bay, we focused on inundation (L) because beach ridge heights (which determine (h)) are comparable, and runup elevations (H) are more variable because most profiles decrease in elevation landward, in some cases to low marshes or river banks. Our reconstruction of paleotsunami runup and inundation may be somewhat underestimated because a tsunami can flow farther landward than its sandy sediments, although it has been shown from post-tsunami surveys that in cases of inundation of less than 2 km, deposits typically reach more than 90% of inundation distance (Abe et al., 2012). In cases of specific tsunami deposits correlated to coseismic subsidence events followed by coastal erosion/retreat, a focus of this paper, inundation distances will be under-represented. This issue is discussed in our analysis.

3. Results

3.1. Profiles and excavations

All three parts of this field area (south, central, north; Fig. 3) are represented by net progradation with some variation (Fig. 11; Electronic Supplement Fig. C1). A trend of net subsidence (possibly excepting southern profiles) is evident from the progressive seaward increase in beach ridge elevation, best shown in profiles 9, 3, 2, 1, 7 and 8 (Fig. 11). Moreover, because the coastal plain is subsiding, there are likely older beach ridges inland, now buried below marsh peat, which can be faintly seen (as drier vegetation) on satellite images. Ages of deposits and of landforms are established by the determined ages of associated tephra. In the north

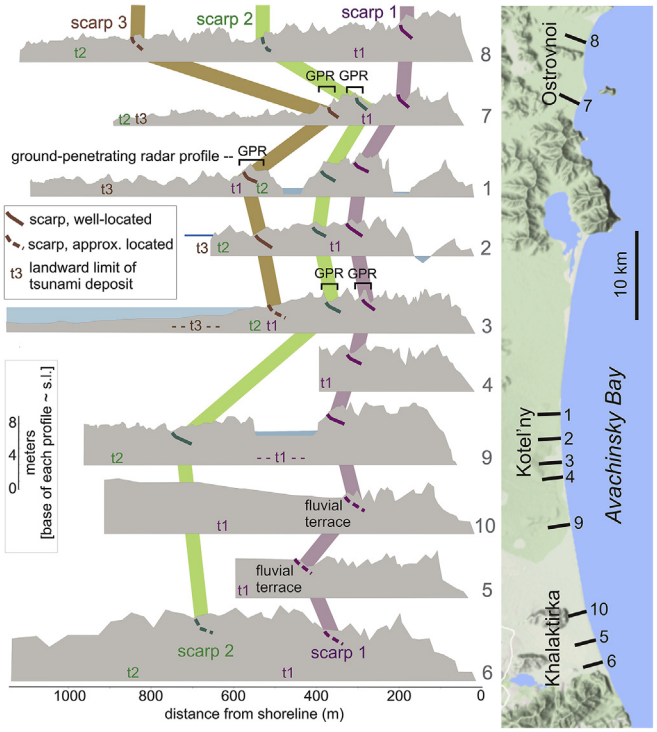

Fig. 11. Simplified plot of 10 measured profiles along Avachinsky Bay north (Fig. 3), with located and correlated buried scarps and their associated tsunami deposits (t1, t2, t3). More details are shown in Electronic Supplement Fig. C1 in Pinegina et al. (2018).

(Ostrovnoi), the oldest ridges with pronounced relief are about 4000 years old, with nearly buried, low-relief older ridges more than 5000 years old. In the middle (Kotel'ny) site the oldest subaerial beach ridges formed ~4000 years ago (Pinegina et al., 2018). In the south (Khalaktirka), only profile 6 has beach ridges older than 1200 years, and this profile is the most disturbed by human activity; on profiles 5 and 10, the wave-built part of the terrace is truncated at a (buried) scarp that cuts into a fluvial terrace. For additional detailed examples of profiles with excavations, see Pinegina et al. (2018).

3.2. Tephra stratigraphy

Excavations in the field area include three well-dated regional marker tephra, two from Ksudach volcano ($KSht_3$ – A.D. 1907, KS_1 – 1800 ^{14}C BP, A.D. 240) and one from the Baraniy Amphitheatre crater, formed at the foot of Opala volcano (OP – 1478 ^{14}C BP, A.D. 606). All are well represented in southern and central Avachinsky Bay sections (Pinegina et al., 2018 and earlier), but only OP is distinctly present in the northern (Ostrovnoi) site, easily recognized due to its stratigraphic position, its contrasting light-pale color, and the presence of visually distinguishable biotite. At the northern site, $KSht_3$ is present as grains in turfy soil, and KS_1 barely present in peat sections and not recognizable in most soil-pyroclastic sections.

A reference section (519) from the central site reported in Pinegina et al. (2018) is correlated here with a peat reference section (857) from the northern site (Figs. 3 and 12; Electronic Supplement Fig. A1). This correlation is aided by radiocarbon dates (ES Table A1), isopach maps (ES Table A3) and geochemical analyses (Electronic Supplement A Text; ES Fig. A4; ES Table B1). The northern site is 29–35 km NE of the central site, twice as far and in a different direction from Avachinsky volcano, thus receiving fewer

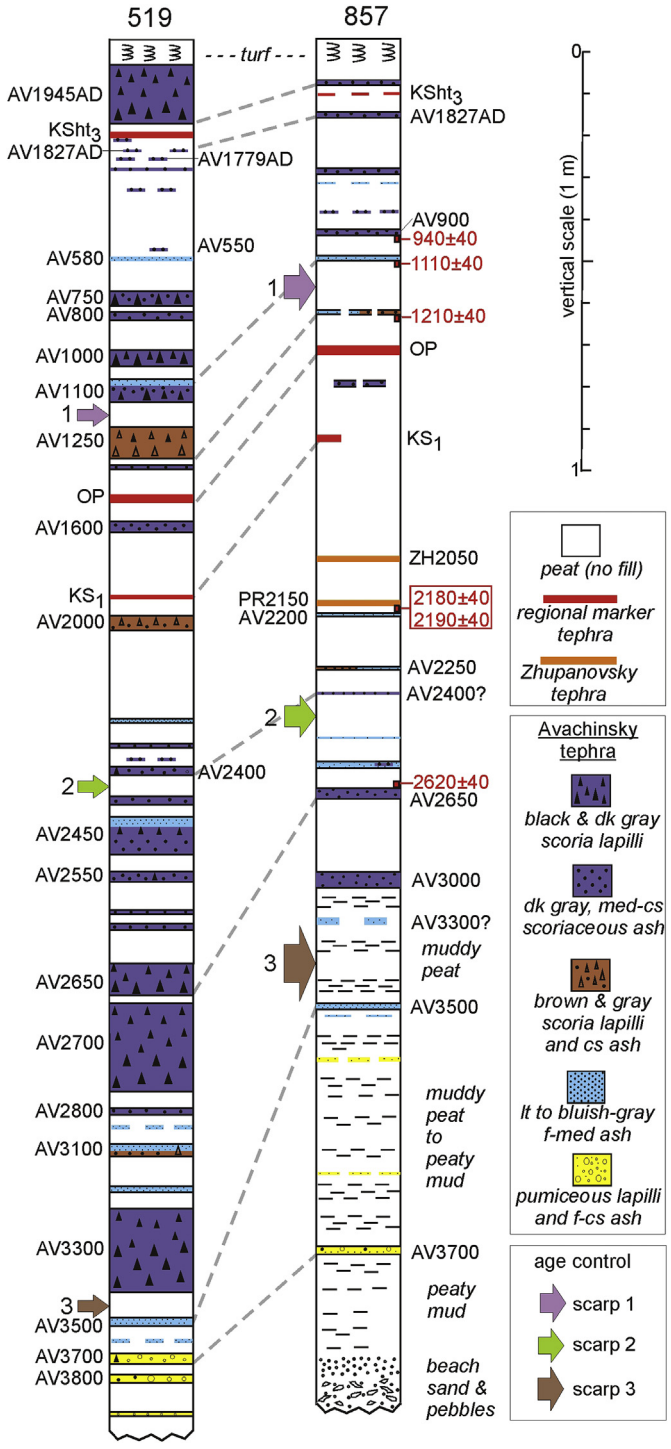

Fig. 12. Reference peat/tephra sections from the central (519) (Pinegina et al., 2018) and northern (857) field sites (located on Fig. 3), with some key correlations shown. New (to this paper) radiocarbon dates in red (Electronic Supplement Table A1). Three buried erosional scarps, S1, S2, S3 – to be discussed in text – are here located (colored arrows) tephrostratigraphically; thickness of arrows gives an indication of degree of age control (discussed in text).

and thinner Avachinsky airfall deposits (Fig. 12). Each site has tephra layers not represented at the other.

The southern (Khalaktirka) site does not have a reference peat section. The best marker tephra present there are $KSht_3$, AV1779AD, AV750, AV1100, OP, KS_1, AV2300, AV2550 and AV3300; tephra from

AV1827AD, AV550 and AV2800 are present in some but not all excavations.

3.3. Buried erosional scarps in Avachinsky Bay

With the help of tephrostratigraphy, we identified and correlated three buried scarps (Fig. 11); scarp S1 was formed ~800 cal AD or ~1100 years ago (1100–1250 ^{14}C years BP), scarp S2, ~600 cal BC or ~2600 years ago (2400–2450 ^{14}C years BP), and scarp S3, ~1700 cal BC or ~3700 years ago (3300–3500 ^{14}C years BP). Also using tephrostratigraphy, we correlated the three buried erosional scarps with associated tsunami deposits t1, t2 and t3 (Fig. 11). From the north through central site, about 50 km, all three scarps and most associated tsunami deposits are present (Fig. 11). Profiles to the south are not old enough to preserve all three scarps, and some profiles are not long enough to preserve all three tsunami deposits. Scarps S1 and S2 have been identified along the entire field area, about 70 km (Fig. 11).

At the (central) Kotel'ny site (Fig. 3), buried erosional scarps are present in the time/tephra intervals AV1100-AV1250, AV2400-AV2450, and AV3300-AV3500 (Fig. 12). At the (northern) Ostrovnoi site, the following markers are used for assigning ages to buried scarps: AV900-OP (~1500 ^{14}C BP), or AV1100-AV1250 (profile 8), AV2250-AV2650, and AV3000-AV3500 (Fig. 12).

Because there are fewer tephra at the northern site, buried scarps there are fixed within longer periods of time than at the central site. We argue that the scarps correlate between the central and northern sites, for which we have more detail, and that Scarps S1 and S2 can be traced to profile 6 in the south for a total distance of 70 km (Fig. 11).

Buried scarp S1. The age of buried scarp S1 is well constrained in the central site and more broadly dated at the northern and southern sites. On (central) Profile 3, scarp S1 cuts into AV1250 and is overlain by AV1100 (Fig. 13). Although these two tephra are present in the northern reference peat section (ES Table A2), only at one point on profile 8 (pt. 817; ES Fig. A5) we detected traces of AV1100 and AV1250, which we used to date and correlate scarp S1. On profile 7, in order to date S1, which still has a topographic expression (Fig. 14) we used AV900 above and the regional marker OP ~1500 ^{14}C BP below (~600 cal yr AD or~1400 cal yr BP). AV900 is traced from the source by an isopach map, with its age previously established near Avachinsky volcano and confirmed by a ^{14}C date

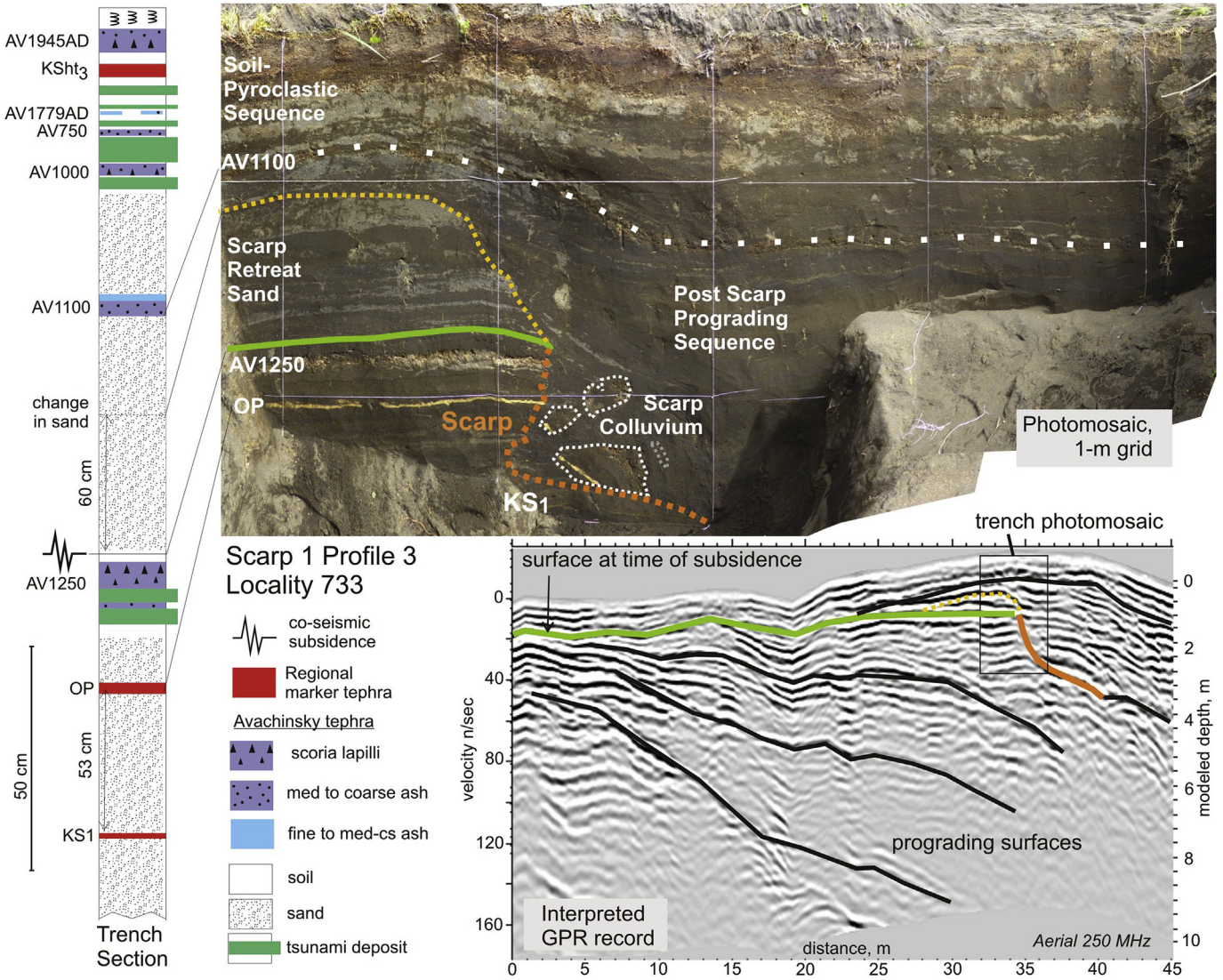

Fig. 13. Buried scarp 1 Profile 3 (located on Fig. 11). Trench photomosaic (1-m grid), composite trench section, and interpreted ground-penetrating radar (GPR) record of buried scarp S1 on Profile 3 in the central (Kotel'ny) field area. Marker tephra (see Fig. 12) are labeled on the section and key tephra are labeled in the photo-mosaic.

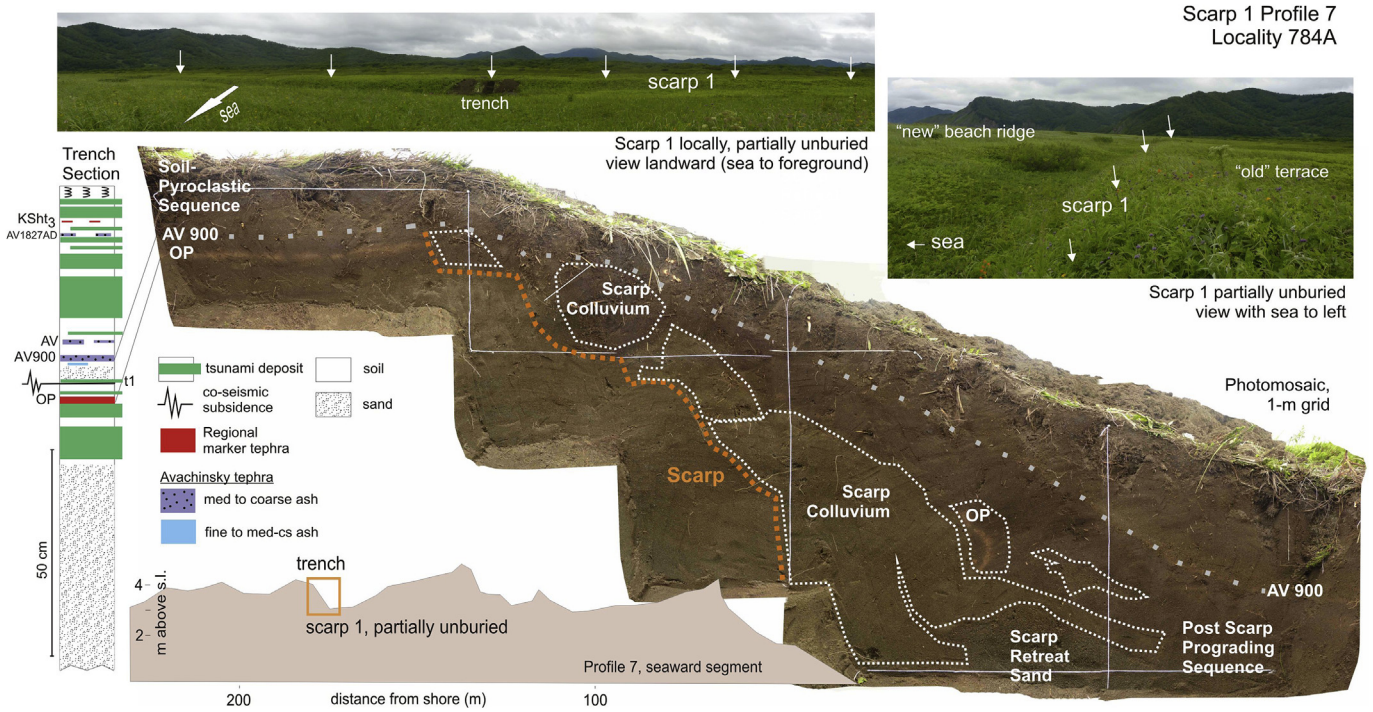

Fig. 14. Partially buried scarp S1 on Profile 7 (see Fig. 11 location). Field photos, trench photo-mosaic (1-m grid), trench section and topographic profile of Scarp 1 on Profile 7, northern (Ostrovnoi) site of Avachinsky Bay. Note that this scarp is still expressed topographically; it is not completely buried. Also note that tsunami deposit t1 is in the section (but not shown in the photo).

obtained from peat section 857 (Fig. 12). On profile 6 in the south, the age of scarp S1 is constrained between AV1100 and OP.

Buried scarp S2. The age of buried scarp S2 is very well constrained on central-site Profile 3 (Fig. 15) between AV2450 and AV2400, the former of which is not present to the north (Profiles 7 & 8), and the latter very thin there (Fig. 12, ex. 857). Thus, for determining the age of the scarp S2 in the north, we use AV2250 and AV2650 (ES Table A2) clearly traced in local tephra sequences. Their stratigraphic position below PR2150 and AV2200 (Fig. 12) helps confirm identification, and both layers can be traced on regional isopach maps and distinguished by coloration and predominance of coarser grains compared to age-proximal thin horizons of tephra (in peat sections, not seen in soil sections). AV2650 identification is also confirmed by ^{14}C dating and volcanic glass study (ES Fig. A4). The age of scarp S2 in the south on profile 6 is constrained to an age between AV2300 and AV2550.

Buried scarp S3. At the central Kotel'ny site, buried scarp S3 cuts into AV3500 and is overlain by AV3300 (Fig. 16), of which AV3500 is easily traced to the north. However, AV3300 is not clear in soil sections in the north, although it appears to be present in peat sections (lenses up to 0.6 cm Gy fine ash) and in individual sections as an admixture in sandy loam. In the absence of a distinctive AV3300 tephra, in order to assign an age to scarp S3 at Ostrovnoi (e.g., Scarp 3 Profile 7, ES Fig. A7), we use AV3000, a dark-gray to ocher-brown, fine to coarse ash 2–4 cm thick, as predicted by its thickness distribution (Bazanova et al., 2005; ES Table A3). Buried scarp S3 is not present or was not identified on profiles at the southern Khalaktirka site because the preserved, prograded coastal plain is too young.

3.4. Subsidence and erosion

3.4.1. Subsidence

The results of applying the three methods (Fig. 10) to estimate the amplitude of what we interpret as coseismic subsidence are shown in Table 1 and Fig. 17 (more complete data in ES Table A4). Note that these measurements are relative to characteristics either side of a scarp (Fig. 10), not relative to sea level. Although the coseismic portion of subsidence may have been added to by post-seismic slip and subtracted from by interseismic uplift, we argue that the coseismic subsidence (as interpreted) generated by these earthquakes accounts for most of the accumulated, net subsidence over time. That is, the subsidence that occurs is permanent. This argument is supported by the net (total) change in each profile elevation (via method 2, Table 1 – excel total profile) as well as by the total of estimated subsidence per profile via each method (Table 1).

There is substantial variation in measurements among profiles for the same scarp, and for measurements via different methods on the same scarp on the same profile; some data are excluded because affected by channel topography. Nevertheless, almost all measurements generate subsidence estimates per event (per scarp) of 0.4–1.2 m (a few smaller or larger), with the net subsidence since scarp S3 (about 3700 years ago) of about 2–2.5 m (Table 1). Methods 1 and 2, which are related in that both use topography (Fig. 10), generate approximately consistent average subsidence for scarps S1 and S2 of 0.5–0.7 m, with scarp S3 ~1 m. The third method (Fig. 10) instead results in a larger average subsidence for Scarp S1 (~1 m), with scarps S2 and S3 ~0.6 m.

The variance in the subsidence-analysis data (Table 1) for the group of central profiles (9, 4, 3, 2, 1), over a short shorewise distance (10 km), and all ~200 km from the trench, is 15% for scarp S1, 7% for S2 and 3% for S3, giving us some confidence in the results. Still, we believe there are too few data points and enough scatter in the data to characterize trends (e.g., systematic change N–S) along Avachinsky Bay or to contrast the three events. There may, however, be a real behavioral difference between profiles 7 and 8, at the north end of the bay, with S2 subsidence larger on Profile 8 and S3

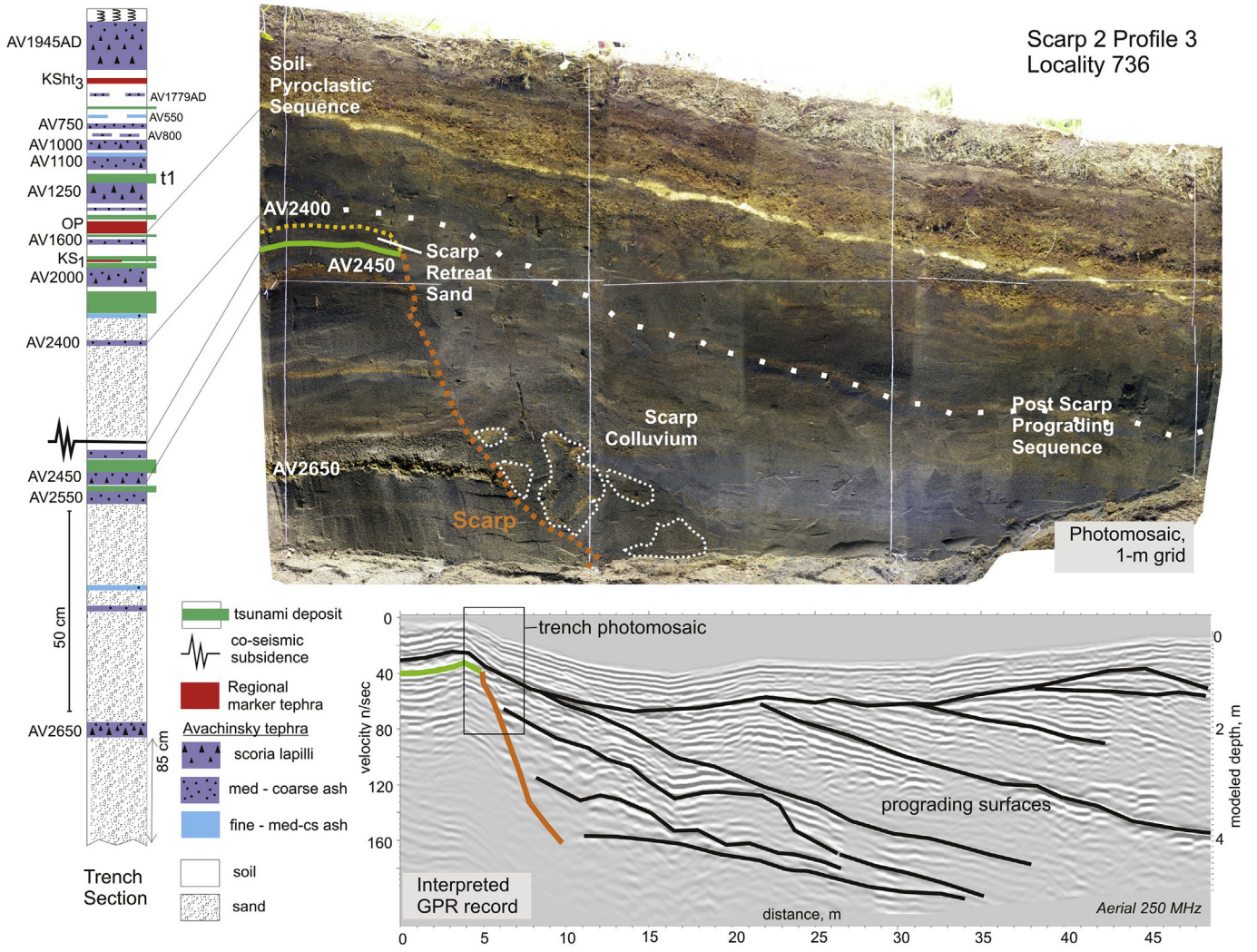

Fig. 15. Buried Scarp S2 on Profile 3, central (Kotel'ny) site (see Fig. 11 location). Trench photo-mosaic (1-m grid), trench section (landward of scarp, correlated to photo) and interpreted GPR record (also see Fig. 7). Note that tsunami deposit t1 is in the section in the soil-pyroclastic sequence above AV1250.

subsidence larger on Profile 7 (Table 1, Fig. 17).

3.4.2. Erosion, progradation and beach-ridge topographies

Using the measured profiles, located scarps and tephra-dated excavations (Fig. 11; ES Fig. C1), we calculated progradation rates and estimated scarp-associated erosion using those rates (Table 2).

Because of differences in sediment supply and wave climate, we used rates specific to each profile, rather than averages among profiles. We used two different ways to calculate short-term rates for time since initiation of progradation after scarp S1 formation – from the shoreline and also from the "**dv**" point (dense vegetation, e.g., Fig. 9). These shorter-term rates are variable, partly due to complexities such as spits and river mouths near the shoreline, with a general trend of more rapid progradation toward the south, more consistent when using the shoreline rather than **dv** (Table 2). All subsequent net progradation rates include whatever erosion might have followed the coseismic subsidence events, as well as other fluctuations. The longest-term rates (**dv** to last excavation; shore to last excavation) are more consistent with each other per profile, but the along-shore trend is more complex, reflecting our finding that some profiles appear to have experienced more event-linked erosion than others.

All profiles with a preserved record between scarps S1 and S2 (therefore quantifiable erosion) show evidence of shoreline retreat following event S1. Profiles 7, 1, 2, 3 and 6 (N to S) show distinct evidence of shoreline retreat (120–280 m, no N–S trend), Profiles 8 and 9 (not in proximity) about 50 m, and on Profiles 5 and 10, scarp S1 has erased any prior accumulative strand-plain material.

There are fewer preserved records between S2 and S3, fewer profiles affected, and smaller calculated erosion amounts, with Profile 8 possibly even showing higher progradation rates (i.e., "negative" erosion) following the S2 event. Profile 7 in the north shows evidence of substantial erosion for both S1 and S2 events, while its neighbor Profile 8 does not. While these two profiles are not far apart, they are separated by a promontory, and as noted above, their subsidence amounts do not necessarily track together (Table 1, Fig. 17).

In addition to locating scarps and estimating progradation and erosion rates/amounts, we counted the number of beach ridges in each profile, the number of ridges between scarps (Table 2), and the nature of the topography associated with each scarp (e.g., Figs. 7, 10, 11, 13–16, A6, A7) compared to other topography (Fig. 11). We made these measurements because it has been suggested that beach ridges may be coseismic indicators (e.g., Kelsey et al., 2015) and that specific beach ridge heights may be indicators of sea level (and thus seismically induced sea-level changes) (e.g., Monecke et al., 2015,

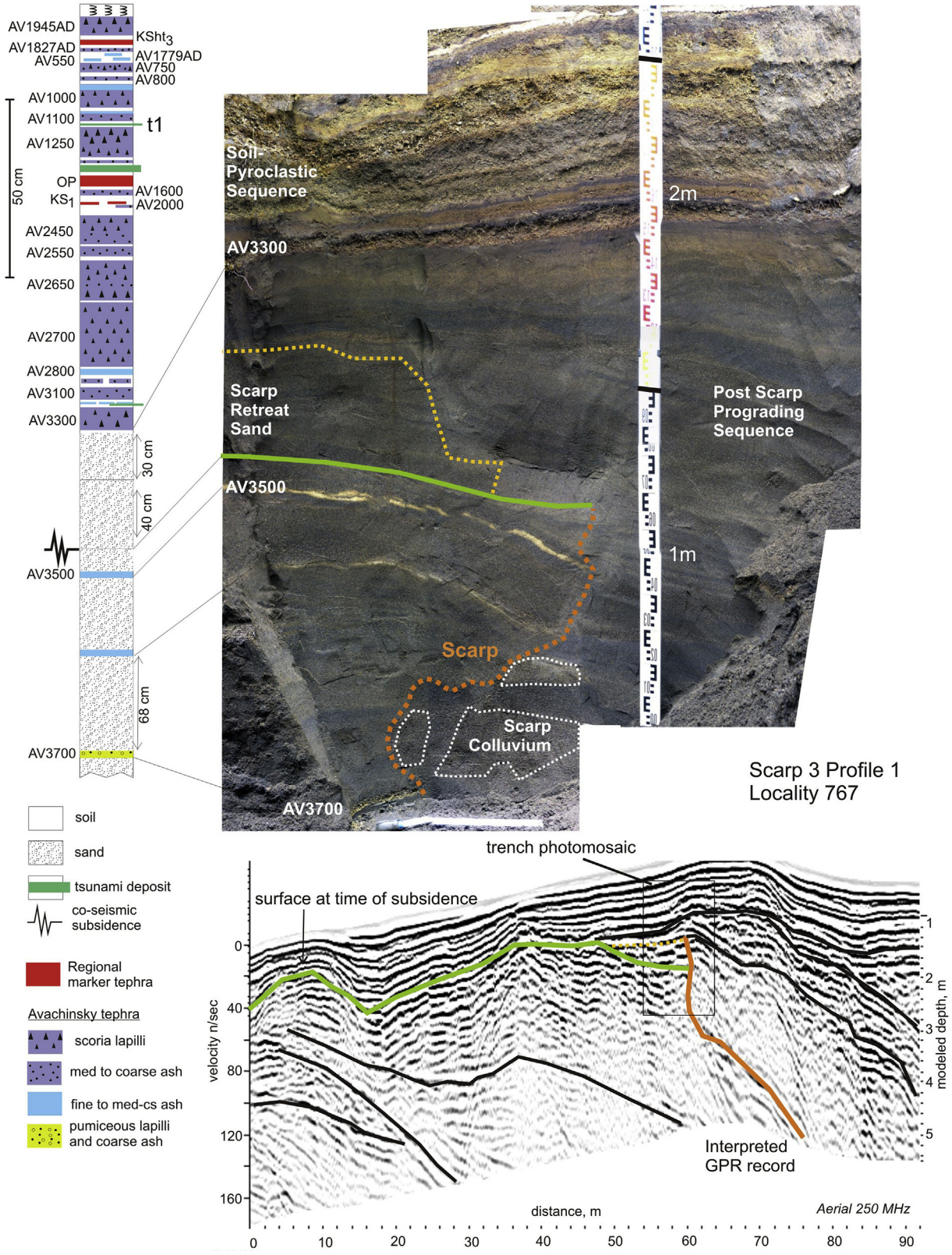

Fig. 16. Buried Scarp S3 on Profile1, central (Kotel'ny) site, Avachinsky Bay (located on Fig. 11). Trench photomosaic, trench section with marker tephra shown and key tephra correlated to the photo, and interpreted GPR record. Note that tsunami deposit t1 is in the section in the soil-pyroclastic sequence above AV1250.

2017). Our basic conclusion is that in the case of Avachinsky Bay, specific, distinct ridges do not correlate with coseismic subsidence events, but there commonly is subdued positive topography generated by the accumulation of scarp-retreat sand. There are

Table 1
Subsidence measurements, in meters, by scarp (color coded) and method (Fig. 10). More complete set of data, including ranges (shown on Fig. 17) and data excluded in analysis, are given in Electonic Supplement Table A4.

	Profile:	8	7	1	2	3	4	9	6	
SCARP										
	Method 1 -- educated eye -- beach ridge elevations plus evaluation									Average
1		0.95	0.65	0.4	0.45	0.2	0.4	1.1	disturbed	0.59
2		0.75	0.3	0.9	0.5	0.55	--	0.6	0.45	0.58
3		0.75	1.55	1.25	0.7	0.8	--	--	--	1.01
	total(3)	*2.45*	*2.5*	*2.55*	*1.65*	*1.55*	--	--	--	*2.14*
	Method 2 -- excel calculations -- average elevation									
1		0.7	0.5	0.7	0.5	0.3	too short	channel*	disturbed	0.50
2		channel*	0.5	channel*	1.2	0.4	--	0.7	0.7	0.70
3		0.5	1.9	0.9	0.9	0.9	--	--	--	1.02
	total(3)	--	*2.9*	--	*2.6*	*1.6*	--	--	--	*2.37*
	excel total profile^	2.9	2.1	2.8	1.5	1.6	--	2.7	2.1	2.24
	maximum age (yr)	4250	4250	4250	3800	3800	--	2800	3300	
	Method 3 -- dv elevation difference in SPS									
1		0.9	0.7	0.9	0.7	1.2	0.8	1.5	disturbed	0.96
2		0.8	0.4	channel*	0.9	0.4	--	0.5	0.3	0.55
3		0.3	0.8	0.7	0.6	0.8	--	--	--	0.64
	total(3)	2.0	1.9	--	*2.2*	*2.4*	--	--	--	*2.13*

*affected by low channel/lagoon -- not used in stats (see Electronic Supplement Table A4)
^excel total profile -- method 2 (Fig. 10) applied from oldest excavation to youngest beach ridge

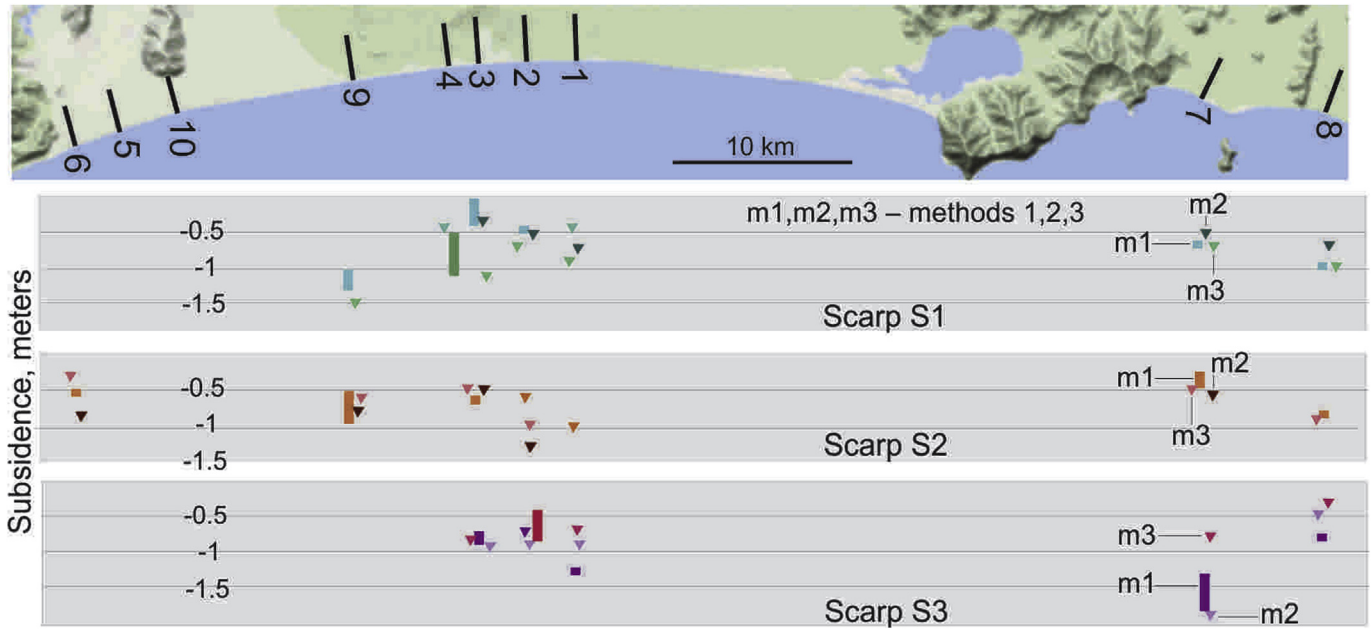

Fig. 17. Summary of estimated coseismic subsidence associated with each scarp event (complete data in ES Table A4, including ranges, which are not shown in Table 1). Triangles are points, lines are ranges. Methods are illustrated in Fig. 10.

many higher ridges on the profiles than there are scarps, and yet fewer ridges than tsunami deposits. These findings and their implications will be covered in more detail in our discussion section.

3.5. Tsunami size

This analysis of tsunami deposits is primarily limited to four profiles with the most detailed study–profiles 1, 3, 7 and 8. Thirty-three tsunami deposits from profiles 1 and 3 (central, Kotel'ny site) were reported and analyzed in Pinegina et al. (2018), of which five are historical (Table 3). Using tephra, we correlated 25 of those 33 tsunami deposits to northern profiles 7 and 8 (Ostrovnoi site, Fig. 3) (Table 3; ES Table D1). For all deposits, we reconstructed paleoshorelines and paleoelevations and calculated sediment inundation (L), sediment runup (H) and maximum beach ridge height seaward of a deposit (h) (ES Fig. A3) (ES Table D1). Because runup is strongly affected by profile elevations inland, which can be quite low, we focus our comparison on L (inundation) because beach ridge height

Table 2
Net progradation rates (m/100yr) and (post-subsidence) erosion calculations (m), per profile, with reference to buried scarps S1,S2, S3 (Fig. 11).

PROFILE:	8	7	1	2	3	4	9	10	5	6	*AVG*
PROGRADATION RATE, net, m/100yr (=cm/yr)											
shore to S1 (1120 yr)	15.9	14.5	25.7	27.3	23.9	29.3	26.8	27.9	38.4	32.7	*26.2*
dv* to S1 (1120 yr)	12.9	11.4	17.1	12.3	18.8	22.7	21.6	18.9	31.3	17.1	*18.4*
dv to S2 (2640 yr)	18.2	8.8	10.3	8.3	11.4	–	23.4	–	–	19.2	*14.2*
dv to S3 (3670 yr)	23.4	8.6	13.2	10.5	12.9	–	–	–	–	–	*13.7*
dv to last exc	24.7	18.4	21.8	11.5	12.2	10.0	26.2	33.4	24.3	33.3	*21.6*
shore to last exc	25.5	19.2	24.1	15.9	13.7	12.6	28.3	40.6	28.8	38.6	*24.7*
AVG:	20.1	13.5	18.7	14.3	15.5	18.6	25.3	30.2	30.7	28.2	
avg short (to S1) minus avg long (to last exc)	−10.7	−5.8	−1.5	6.1	8.4	14.7	−3.0	−13.6	8.3	−11.1	
PROGRADATION RATE per interval of subsidence and erosion, m/100yr (=cm/yr)											
S1 to S2 (1520 yr) [S1 erosion]	22.1	6.8	5.3	5.4	5.9	–	24.7	–	–	20.7	*13.0*
S2 to S3 (1030 yr) [S2 erosion]	30.7	6.0	17.1	13.2	13.6	–	–	–	–	–	*16.1*
EROSION ESTIMATE (m) = (expected distance^) - (actual distance)											
S1 to S2 [S1 erosion]	51.0	187.1	286.2	159.6	118.8	–	53.5	–	–	272.8	*161.3*
S2 to S3 [S2 erosion]	−53.8	135.3	72.2	27.7	1.5	–	–	–	–	–	*36.6*
NUMBER OF BEACH RIDGES											
since S1 (to present)	4	4	5–6	5–6	9–11	6–7	4–5	5–7	8–9	3–4	
S1 to S2	7–13	4–5	2–4	3	2–3	–	5–6	–	–	3–6	
S2 to S3	7–12	3–4	1–3	4	1–3	–	–	–	–	–	

*dv = first dense vegetation from shore inland (e.g., Fig. 9).
^expected distance (m) = time elapsed x net rate shore to last excavation.

Table 3
Reconstructed parameters (inundation, L, in m; ridge height, h, in m) of historic and prehistoric tsunamis on the northern (8,7) and central (1,3) Avachinsky Bay coast, including marker tephra layers, but excluding scarp-retreat erosion estimates (see text for discussion).

cum 7&8	cum 1&3	Corr N - > S	Type of Layer	Profile 8		Profile 7		Profile 1		Profile 3		*Avg* L
				L	h	L	h	L	h	L	h	AvgL_all
1	*1*	1	Tsunami 1952	**172**	**4.6**	**176**	**4.8**	**210**	**4.7**	**150**	**5.5**	**177**
2	*2*	**2**	**Tsunami 1923** KSht3	**217**	**4.6**	**283**	**4.8**	**210**	**4.7**	**190**	**5.5**	**225**
3	*3*	**3**	**Tsunami 1841** AV1827AD	**172**	**4.6**	**172**	**4.8**	**210**	**4.7**	**270**	**5.5**	**206**
4	*4*	**4**	**Tsunami 1792**	**118**	**4.6**	**180**	**4.8**	**310**	**5.7**	**270**	**5.5**	**220**
5	*5*	**5**	**Tsunami 1737**	**118**	**4.6**	**113**	**4.8**	**210**	**4.7**	**210**	**5.5**	**163**
6	*6*	**6**	**Ts~1400–1700 AD**	**326**	**4.6**	**317**	**4.8**	**460**	**5.7**	**300**	**5.7**	**351**
7	*7*	7	Tsunami			232	4.3	120	5.5	150	5.5	167
10	*10*	10	Tsunami			2 km r[a]	river[a]	285	5.7			
11	*12*	**12**	**Ts Scarp S1 = t1**	**110**	**4.3**	**96**	**4.3**	**315**	**5.7**	**220**	**5.7**	**185^**
12	*14*	**14**	**Tsunami** OP	**196**	**4.3**	**179**	**4.3**	**350**	**5.7**	**220**	**5.7**	**236**
14	*15*	**15**	**Tsunami**	**355**	**4.3**	**321**	**4.2**			**190**	**5.7**	**289**
15	*16*	**16**	**Tsunami** KS1 or AV ~ KS1	**429** AV	**4.3**	**463** AV	**4.2**	**315** KS1	**5.7**	**190** KS1	**5.7**	**349**
16	*17*	**17**	**Tsunami**	**355**	**4.3**	**428**	**4.2**	**175**	**4.7**	**200**	**5.7**	**290**
17	*18*	18	Tsunami	196	4.3					120	5.7	158
18	*19*	**19**	**Ts Scarp S2 = t2**	**500**	**3.8**	**715**	**4.2**	**175**	**4.7**	**200**	**5.7**	**397^**
19	*20*	**20**	**Tsunami** AV2650	**186**	**3.8**	**458**	**4.2**	**175**	**4.7**	**130**	**5.7**	**237**
20	*25*	25	Tsunami			355	4.1	180	4.7	120	5.2	218
21	*26*	26	Tsunami			325	4.1	175	4.7	560r[a]	5.3[a]	250
22	*27*	27	Tsunami			118	3.4			560r[a]	5.3[a]	
23	*28*	**28**	**Tsunami**			**399**	**3.4**	**265**	**4.7**	**560r**[a]	**5.3**[a]	**332**
24	*30*	**30**	**Ts Scarp S3 = t3** AV3500			**551**	**3.4**	**425**	**4.3**	**lake**[a]	**5.3**[a]	**488**
25	*31*	**31**	**Tsunami** AV3700			**551**	**3.4**	**196**	**4.3**			**374**
27	*32*	**32**	**Tsunami** AV3800			**532**	**3**			**lake**[a]	**4.7**	
28	*33*	**33**	**Tsunami**			**494**	**3**	**365**	**4.3**			**430**
			AVERAGES	**243**	**4.4**	**332**	**4.1**	**251**	**5.0**	**197**	**5.6**	**269^**

Notes.
Distances calculated from paleo-dv, then a beach width is added based on specific modern profile.
L = farthest distance from dv with tsunami deposit; h = elevation of highest point seaward of L (ES Fig. A3).
Bold indicates more confident correlation; ordinal numbers were assigned to profiles 1 & 3 (Pinegina et al., 2018) then correlated with deposits on profiles 7 & 8; only 25 of 33 deposits were correlated; see ES Table D1.
^See text discussion with regard to post-tsunami scarp retreat/erosion, which would increase these numbers.
[a] Deposits that either ran into lakes/lagoons or traveled up rivers were not used in statistics and comparisons.

does not vary much among profiles (Table 3), and H (runup) is highly variable due to elevations at the landward ends of profiles (Fig. 11) (ES Table D1).

On all ten profiles, in excavations landward of a buried scarp, we identified and described tsunami deposits which had the same stratigraphic age as scarp events and mapped their distribution (t1, t2, t3, Fig. 11, Table 3, Table 4). For scarp tsunamis t1 and t2, we then reconstructed inundation where possible by adding back calculated erosion (Table 2, Table 4). Such a correction should not be necessary for non-scarp-correlated tsunami deposits because their inundation is calculated from a paleo-dv, which will be from the profile once it has turned around to progradation.

While scarp-tsunami t1 sediment inundation (L) appears relatively small when not accounting for erosion, adding estimated erosion places it, along with t2 and t3, in the group of largest tsunamis (in terms of L) in the last 4000 years (Table 3). The average L of the (uncorrected) averages per profiles 8, 7, 1 and 3 (Table 3) is 269 m, with seven of the 25 correlated tsunami deposits >25% larger than the average, including t2 and t3. Erosion-corrected inundation distances for t1 and t2 change the *average* very little (to 280 m), but move t1 into the larger-than-25% (>350 m average) group with the following order, larger to smaller: **t3**, **t2**, 33, 31, **t1**, 6 (Ts~1400-1700AD) and 16. In either case, corrected or not, tsunami deposit t2, correlated with Scarp S2, is distinctly larger in the north.

4. Discussion and conclusions

In the last 4000 years, the geological record of the Avachinsky Bay strand plain contains evidence for about ten times more large tsunamis (runup >5 m) than for events with coseismic subsidence sufficient to result in distinct erosional scarps, as well as with offshore deformation sufficient to generate large tsunamis. What is the nature of these millennial earthquakes?

4.1. Comparison among paleoseismic events 1, 2 and 3

The three buried scarps on the Avachinsky Bay coastal plain can be correlated alongshore for 10s of kms and are each thus related to single events. From central Profile 3 northward, over a distance of about 50 km, all three buried scarps have been located on each of five profiles and are well-located in 12 out of 15 cases (Fig. 11). Scarps 1 and 2 are also located approximately and age-constrained moderately on the southernmost profile 6, for a total alongshore distance (profile 6 to profile 8) of about 70 km. The age constraints for each scarp are on the order of 100 years, whereas the age span between scarps is 1000–1500 years. Moreover, within the same tephra-age constraints of each scarp, there is also a tsunami deposit.

Although events 1, 2 and 3 are unusual in the local paleoseismic record, they are similar to each other. Events 1 and 2 can be compared more completely; we do not have enough information older than Event 3 to calculate time lapse since the prior event, or to quantify post-subsidence erosion. Event 1 occurred after a longer time lapse (~1500 yr) than Event 2 (~1000 yr). Scarp-associated erosion (coastal retreat) appears to have been more in Event 1 (average 160 m) than in Event 2 (average 40 m) (Table 2).

With regard to net subsidence as determined by our methods, all three events have similar averages (~0.5–1.0 m; Table 1), Event 3 possibly slightly more. The determinations vary (Fig. 17), but overall the data appear to be reasonable, e.g., compared to measured and modeled deformation in Chile 2010 (Moreno et al., 2012) and Tohoku 2011 (Kobayashi et al., 2011).

The tsunamis associated with the buried scarps are all larger than the five historical tsunamis and among the largest in last 4000 years (Table 3); t3 may have been particularly large. Because runup elevation (H) and maximum beach-ridge elevation (h) are quite variable on these profiles, we used inundation distance (L) as our comparator of tsunami size. However, post-subsidence erosion and coastal retreat can have a significant effect on determining inundation distances. Because of the large amount of erosion indicated for event 1, for example, its actual tsunami inundation distance (average 340 m, from Table 4), would have been significantly larger than measured (average 185 m, Table 3) without an erosion correction.

4.2. Alongshore variations for each event

With regard to alongshore variations, the data are not highly consistent, but with some possible trends. The total distance alongshore is 70 km, and the difference in distance from the trench 20 km: ~180 km for profiles 7 and 8, ~200 km for the rest. Based on historical examples, as well as modeling, variations can be expected in subsidence amounts, erosion rates/amounts, and tsunami size.

The subsidence amounts we quantify do not indicate significant alongshore differences or trends (Table 1, Fig. 17), and the data are variable, but indicate subsidence on the order of 1 m in all three events. We might predict that the northern profiles 7 and 8 would show differences compared to central and southern profiles because they are farther from others (40–70 km alongshore) and somewhat closer to the trench. However, there is more variation in subsidence between 7 and 8 than there is compared to other profiles, particularly for events 2 and 3. This variation may be explained by more local faulting associated with nearby Shipunsky Peninsula, interpreted as a tectonic boundary (Lander and Shapiro, 2007).

The alongshore variation in event-associated erosion is quite

Table 4
Measured and calculated tsunami sediment inundation (L) for scarp-associated tsunamis t1, t2 and t3.

PROFILE:	8	7	1	2	3	4	9	10	5	6
Calculated tsunami inundation (m) = measured distance + calculated erosion[a] + 50 m beach width										
t1 scarp S1	211	307	596	250	319	*>90**	<345	*>310**	*>180**	121
t2 scarp S2	496	785	292	298	>252	–	*>220**	n/d	n/d	*>200**
t3 scarp S3	n/d	*>520**	*>390**	*>120**	into lake	–	–	–	–	–
Measured distance (m) = tsunami sediment inundation (L) distance (meters) from mapped scarp										
t1 scarp S1		110	70	260	40	150	*40*	<270 (peat bog)	*260*	*130*	50
t2 scarp S2		500	600	170	220	>200 (lake)	–	*170*	–	–	*150*
t3 scarp S3		soil too compact	470	340	70	>40 (lake)	–	–	–	–	–
Calculated erosion (meters)^										
scarp S1 erosion		51	187	286	160	119		25			21
scarp S2 erosion		−54	135	72	28	2					

^ = expected distance(net progradation shore to last excavation x time interval) - actual distance between scarps (Table 2).
[a] Italic - calculation using only scarp position +50 m active beach (erosion = 0 as unknown).

variable and shows only a weak trend of more erosion in the center of the bay (but also profile 7 and not profile 4) (Table 2), where there are also lower progradation rates. In general greater subsidence predicts more erosion (as per Bruun's rule), but along a 70-km-long bay, other factors such as sediment supply and wave climate are also important. We find no strong correlation between the amounts of subsidence (Table 1) and erosion (Table 2).

Of the four profiles with detailed paleotsunami determinations (Table 3) there is consistency in tsunami inundation between adjacent profiles (northern 7 and 8; central 1 and 3). Generally, inundation is longer on northern profiles, particularly in the older record. Central profiles 1 and 3 are topographically higher than northern Profiles 7 and 8, so the central profiles tend to have higher h (high point seaward of deposit) and shorter L (inundation) (Table 3); runup (H) is difficult to compare because the profiles usually decrease in elevation inland. Tsunami t1 is larger in the central zone, whereas t2 larger in the north. The difference in inundation patterns between the two zones may be useful in (paleo)tsunami modeling.

4.3. Beach ridges are not reliable paleoseismic indicators

Clearly most beach ridges globally are not indicators of earthquake events. There are many beach-ridge plains in the world with innumerable shore-parallel beach (and dune) ridges not associated with earthquakes and coseismic land-level change. The most common factors in their formation are interpreted as related to weather and climate, including storm waves and wind, as well as sediment supply (reviewed in Tamura, 2012). Tamura (2012) cautions using beach ridges as sea-level indicators, particularly because their height is commonly affected by the growth of foredune ridges. When can beach-parallel ridges be used reliably to indicate paleoseismic events?

Stair-step series of beach ridges each stranded by coseismic uplift have been documented in several regions, e.g., New Zealand (McSaveney et al., 2006), Chile (Bookhagen et al., 2006) and Kamchatsky Peninsula (Pinegina et al., 2013). Ridge heights are not related to the uplift, but rather are paleotopography. These cases represent 1) coseismic uplift stranding a surface formerly associated with the shoreline, and 2) net uplift, preserving the coastline topography (with later potential modifying effects of erosion or of wind-generated accumulation). Still, not every ridge in a series like this need be from coseismic uplift.

Saltonstall and Carver (2003) and Kelsey et al. (2015) document historical (1964) and prehistoric beach ridges associated with coseismic subsidence along the Alaska subduction zone. In these cases, post-subsidence erosion led to an accumulation of shore-retreat sand or gravel (a "retreat ridge"), and this accumulation was stranded by post-seismic recovery or uplift. Thus, a shoreline experiencing coseismic subsidence but net long-term stasis or uplift may preserve coseismic beach ridges. Both the Alaska cases, however, are not along broad accumulative strand plains with multiple beach ridges, but rather are in local embayments. Kelsey et al. (2015) note that their interpreted coseismic ridges have steeper sides facing the ocean, indicative of erosional retreat. Indeed, this retreat represents the same process that generated now-buried scarps (and shore-retreat sand) in Avachinsky Bay and elsewhere.

The two cases of broad beach-ridge plains where buried scarps have been identified and correlated with coseismic subsidence are Cascadia's Columbia littoral cell (Meyers et al., 1996; Peterson et al., 2010) and Avachinsky Bay (this study); ongoing work in Chile may add to these examples (M. Cisternas, written communication). Both the Avachinsky-Bay and Columbia-cell locations are undergoing net subsidence. In neither case do beach ridges correlate with identified paleoseismic events indicated by buried scarps. In the Cascadia example, there are more scarps than there are beach or foredune ridges; scarps and ridges are not co-located; ridge heights are related to eolian processes. Phipps et al. (2001) interpreted one ridge, the "big dune," to have been reactivated after A.D. 1700 coseismic subsidence. On the Avachinsky beach-ridge plain, there are many more beach ridges on the strand plain than scarps, but fewer ridges than tsunami deposits; beach ridges proximal to scarps are not distinctive–there are many higher ridges. Clearly beach ridges in these two cases cannot be used as paleoseismic indicators.

Will coseismic subsidence and shore retreat leave behind a higher-than-usual ridge? Monecke et al. (2015) make this case for the Aceh coast–where there are multiple beach ridges, they assign coseismicity to the two highest. In the aforementioned Alaska cases, the answer may be "yes", but there are no other ridges to compare them to. The answer is "no" in Avachinsky Bay and along the Columbia littoral cell of Cascadia. Net subsidence in these cases has resulted in higher ridges closer to the shoreline, in any case, as older ridges experience more time of net subsidence. As to ridge-swale relief, there are too many factors involved, particularly eolian processes and inter-ridge erosion, so relief is an unreliable indicator of sea-level change. Particularly in the Avachinsky Bay case, where many ridges have highly variable relief (Fig. 11, ES Fig. C1), ridge height or relief cannot be attributed to sea-level changes on the ridge-by-ridge time scale.

In sum, shorelines undergoing net uplift or stasis may preserve shoreline topography associated with seismic events, or otherwise stranded by uplift. However, shorelines undergoing net subsidence are not expected to preserve distinct ridges associated with seismic events.

4.4. Comparing Kamchatka's Avachinsky Bay to Cascadia's columbia littoral cell

We can contrast the rarity of coseismic subsidence events in Avachinsky Bay with the case of the aforementioned Columbia River littoral cell along the Cascadia subduction zone. Both strand plains comprise sets of prograded sandy beach ridges on the order of 5 m high, progradation rates of 2–4 m/100 yr, and net subsidence resulting in topographic profiles that rise toward the shore. Yet in this part (Columbia littoral cell) of Cascadia *every* earthquake documented by buried soils and tsunami deposits appears to have a correlative buried scarp as identified on GPR and dated with radiocarbon (Meyers et al., 1996; Peterson et al., 2010). That is, every great earthquake generates coseismic subsidence in the onshore coastal zone on the order of 1 m (at the Columbia cell latitude).

Recurrence intervals in the two cases are distinctly different. The recurrence intervals for great (Mw > 8) earthquakes along the Kamchatka subduction zone is less than 100 years, and of Mw > 9 events on the order of 200 years, with some along-trench variation (Pinegina, 2014). The Cascadia subduction zone in the region of the Cascadia littoral cell has a recurrence interval of great earthquakes in the range of 500–600 yr (Atwater and Hemphill-Haley, 1997). In terms of possible segmentation, southern Kamchatka (south of Shipunsky Peninsula, Fig. 3) tends to rupture in larger, less frequent events than northern Kamchatka, both historically and prehistorically, with the prehistoric record based on paleotsunami studies (Pinegina et al., 2018; Bourgeois and Pinegina, 2018). The nature and evidence of segmentation of the full Cascadia subduction zone is recently summarized by Bodmer et al. (2018); the recurrence interval of Cascadia earthquakes may be shorter toward the south (e.g., Witter et al., 2013) and longer in the north (Hutchinson and Clague, 2017).

In terms of historical analogues of tsunamigenic earthquakes in the two cases, the 1952 Mw ~9 Kamchatka earthquake ruptured as far north as Shipunsky, but the rupture appears to have been concentrated farther south (MacInnes et al., 2010); there is not a record of 1952 coseismic subsidence in Avachinsky Bay, which is at the northern limit of the southern Kamchatka zone (Fig. 1). Cascadia subduction-zone earthquakes have no local historical record; the A.D. 1700 event is dated historically and quantified as Mw ~9 by the tsunami arriving in Japan (Satake et al., 2003). This A.D. 1700 event has a well-established coastal stratigraphic record, including evidence of coseismic subsidence and a tsunami (Event Y of Atwater and Hemphill-Haley, 1997).

There are many geophysical/geodynamic differences between Cascadia and Kamchatka subduction zones, which are expressed, e.g., in earthquake frequency and volcanic activity, Kamchatka being more active. One difference that may help explain the rarity of onshore coseismic subsidence in Avachinsky Bay is its distance from the trench (180–200 km), compared to the Columbia River strand plain (~100–110 km). Moreover, the Kamchatka subduction zone at this latitude has a slab dip of ~30° at the shoreline and an ~80-Ma Pacific crust subducting more-or-less orthogonally at a rate of ~80 mm/yr. The Cascadia subduction zone at the latitude of SW Washington has a slab dip of ~11.5° at the shoreline and a ~10-Ma Juan de Fuca crust subducting obliquely at a rate of ~40 mm/yr (Hayes et al., 2012). Thus, the seismogenic ("locked") zone in the Cascadia case should be wider, and therefore coseismic subsidence would more commonly reach the coastal zone.

Coseismic subsidence on the order of 200 km from a trench requires either a very wide subduction-zone rupture (e.g., Fig. 2), or rupture of only the deeper part of the seismogenic zone. Because these Kamchatka cases (coseismic subsidence associated with scarps S1, S2, S3) can be correlated with large tsunamis, water-displacing deformation offshore is required, making the very-wide case most likely. Along Avachinsky Bay, these wide ruptures are the exception in the last 4000 years, with other tsunamigenic earthquakes not generating noticeable onshore subsidence, that is, with most (if not all) coseismic, tsunamigenic deformation occurring offshore.

4.5. Conclusions

With unprecedented detail, we have examined the geologic evidence of three unusually wide subduction-zone-earthquake ruptures each characterized by coastal coseismic subsidence, offshore deformation generating large tsunamis, subsidence-consequent erosional retreat of the coastline, and then a return to coastal progradation. This paper represents the first time buried erosional scarps have been documented not only with detailed ground penetrating radar (GPR) records but also with trench excavations and with tephrostratigraphy that permits correlation of the scarps and associated tsunami deposits along the coast. We also have used stratigraphic methods to quantify the amount of subsidence, tsunami size, and erosional retreat for each of these events. Particularly with regard to subsidence, we have developed new methods to estimate coseismic land-level change in a case where flora and fauna are absent from the record.

Although the Kuril-Kamchatka subduction zone is one of the most active in the world, there are no historical analogues for these three events. Indeed, they are a rarity on a subduction zone experiencing large, tsunamigenic earthquakes every 125 years average in the last 4000 years. Thus, these events provide insight into the range and millennial-scale variability of subduction-zone behavior.

CRediT authorship contribution statement

T.K. Pinegina: Conceptualization, Funding acquisition, Project administration, Investigation, Methodology, Writing - original draft, Writing - review & editing. **J. Bourgeois:** Conceptualization, Investigation, Methodology, Formal analysis, Writing - original draft, Writing - review & editing. **L.I. Bazanova:** Investigation, Methodology, Formal analysis, Writing - original draft, Writing - review & editing. **E.A. Zelenin:** Formal analysis, Software. **S.P. Krasheninnikov:** Formal analysis, Data curation. **M.V. Portnyagin:** Data curation, Writing - review & editing.

Acknowledgments

Field research was supported by grants from the Russian Foundation for Fundamental Research #15-05-0265, #18-05-00407 & from Far East Branch of Russian Academy of Sciences #18-5-003 (to T. Pinegina). Research and manuscript preparation were partly supported by Russian Ministry of Education and Science (grant N 14.W03.31.0033 to N. Shapiro) and by state scientific program #0282-2018-0019 (to IViS FEB RAS). We are very grateful to Andrey Kozhurin, who generated the photomosaics of the trenches, which he helped to dig; we also thank Danil Vidrin and Anton Khomchanovsky for their field assistance. We are deeply grateful to Vera Ponomareva for her oversight in tephra analysis and her review of the manuscript and data, Alexander Lander for many discussions, and Bre MacInnes for critical notes and manuscript review. We thank two anonymous reviewers for their constructive feedback.

Appendix A. Supplementary data

Supplementary data to this article can be found online at https://doi.org/10.1016/j.quascirev.2020.106171.

References

Abe, T., Goto, K., Sugawara, D., 2012. Relationship between the maximum extent of tsunami sand and the inundation limit of the 2011 Tohoku-oki tsunami on the Sendai Plain, Japan. Sediment. Geol. 282, 142–150.

Ando, M., 1975. Source mechanisms and tectonic significance of historical earthquakes along the Nankai Trough, Japan. Tectonophysics 27 (2), 119–140.

Arcos, M.E.M., 2012. The AD 900–930 Seattle fault zone earthquake with a wider coseismic rupture patch and postseismic submergence: inferences from new sedimentary evidence. Bull. Seismol. Soc. Am. 102 (3), 1079–1098.

Atwater, B.F., Hemphill-Haley, E., 1997. Recurrence Intervals for Great Earthquakes of the Past 3,500 Years at Northeastern Willapa Bay. Washington, U.S. Geological Survey Professional Paper 1576.

Bodmer, M., Toomey, D.R., Hooft, E.E., Schmandt, B., 2018. Buoyant asthenosphere beneath Cascadia influences megathrust segmentation. Geophys. Res. Lett. 45 (14), 6954–6962.

Barrientos, S.E., Ward, S.N., 1990. The 1960 Chile earthquake: inversion for slip distribution from surface deformation. Geophys. J. Int. 103, 589–598.

Bazanova, L.I., Braitseva, O.A., Dirksen, O.V., Sulerzhitsky, L.D., Danhara, T., 2005. Ashfalls from the largest Holocene Eruptions along the Ust'-Bol'sheretsk – Petropavlovsk-Kamchatsky traverse: sources, chronology, recurrence. J. Volcanol. Seismol. 6, 30–46.

Bookhagen, B., Echtler, H.P., Melnick, D., Strecker, M.R., Spencer, J.Q., 2006. Using uplifted Holocene beach berms for paleoseismic analysis on the Santa María Island, south-central Chile. Geophys. Res. Lett. 33 (15) https://doi.org/10.1029/2006GL026734.

Bourgeois, J., Pinegina, T.K., 2018. The 1997 Kronotsky earthquake and tsunami and their predecessors, Kamchatka, Russia. Nat. Hazards Earth Syst. Sci. 18 (1), 335–350.

Braitseva, O.A., Ponomareva, V.V., Sulerzhitsky, L.D., Melekestsev, I.V., Bailey, J., 1997a. Holocene key-marker tephra layers in Kamchatka, Russia. Quat. Res. 47 (2), 125–139.

Braitseva, O.A., Sulerzhitsky, L.D., Ponomareva, V.V., Melekestsev, I.V., 1997b. Geochronology of the greatest Holocene explosive eruptions in Kamchatka and their imprint on the Greenland glacier shield. *Transactions (Doklady) of the Russian Academy of Sciences*. Earth Sci. Sect. 352 (1), 138–140.

Bristow, C.S., Jol, H.M. (Eds.), 2003. Ground Penetrating Radar in Sediments. Geological Society of London.

Bruun, P., 1962. Sea-level as a cause of shore erosion. J. Waterw. Harb. Div. ASCE 88, 117–130.
Bürgmann, R., Kogan, M.G., Levin, V.E., Scholz, C.H., King, R.W., Steblov, G.M., 2001. Rapid aseismic moment release following the 5 December, 1997 Kronotsky, Kamchatka, earthquake. Geophys. Res. Lett. 28 (7), 1331–1334.
Buynevich, I.V., FitzGerald, D.M., Goble, R.J., 2007. A 1500 yr record of North Atlantic storm activity based on optically dated relict beach scarps. Geology 35 (6), 543–546.
Cisternas, M., Mizobe, C., Wesson, R., Ely, L., Muñoz, A., Dura, T., Melnick, D., 2017. Beach ridges, buried erosional scarps and overhanging soils evidence recurring past co-seismic subsidence midway along the area of the giant 1960 Chile earthquake. Geol. Soc. Am. Abstr. tProgr. 49 (6) https://doi.org/10.1130/abs/2017AM-302380. ISSN 0016-7592.
Crowell, A.L., Mann, D.H., 1996. Sea level dynamics, glaciers, and archaeology along the central Gulf of Alaska coast. Arctic Anthropol. 33 (2), 16–37.
Dura, T., Hemphill-Haley, E., Sawai, Y., Horton, B.P., 2016. The application of diatoms to reconstruct the history of subduction zone earthquakes and tsunamis. Earth Sci. Rev. 152, 181–197.
Dura, T., Horton, B.P., Cisternas, M., Ely, L.L., Hong, I., Nelson, A.R., Wesson, R.L., Pilarczyk, J.E., Parnell, A.C., Nikitina, D., 2017. Subduction zone slip variability during the last millennium, south-central Chile. Quat. Sci. Rev. 175, 112–137.
Farías, M., Vargas, G., Tassara, A., Carretier, S., Baize, S., Melnick, D., Bataille, K., 2010. Land-level changes produced by the Mw 8.8 2010 Chilean earthquake. Science 329 (5994), 916-916.
Gusev, A.A., 2004. The schematic map of the source zones of large Kamchatka earthquakes of the instrumental epoch. In: Complex Seismological and Geophysical Researches of Kamchatka. To 25th Anniversary of Kamchatkan Experimental & Methodical Seismological Department", Ed. By Gordeev E.I., Chebrov V.N. Petropavlovsk-Kamchatsky, p. 445 (in Russian).
Gusev, A.A., Shumilina, L.S., 2000. Modeling the intensity–magnitude–distance relation based on the concept of an incoherent extended earthquake source. J. Volcanol. Seismol. 21, 443–463.
Gusman, A.R., Tanioka, Y., Sakai, S., Tsushima, H., 2012. Source model of the great 2011 Tohoku earthquake estimated from tsunami waveforms and crustal deformation data. Earth Planet Sci. Lett. 341, 234–242.
Hashima, A., Becker, T.W., Freed, A.M., Sato, H., Okaya, D.A., 2016. Coseismic deformation due to the 2011 Tohoku-oki earthquake: influence of 3-D elastic structure around Japan. Earth Planets Space 68 (1), 1–15, 159.
Hayes, G.P., Wald, D.J., Johnson, R.L., 2012. Slab1.0: a three-dimensional model of global subduction zone geometries. J. Geophys. Res. 117, B01302. https://doi.org/10.1029/2011JB008524.
Hutchinson, I., Clague, J., 2017. Were they all giants? Perspectives on late Holocene plate-boundary earthquakes at the northern end of the Cascadia subduction zone. Quat. Sci. Rev. 169, 29–49.
Imakiire, T., Koarai, M., 2012. Wide-area land subsidence caused by "the 2011 off the pacific coast of Tohoku earthquake". Soils Found. 52 (5), 842–855.
Johnson, J.M., Satake, K., 1999. Asperity distribution of the 1952 great Kamchatka earthquake and its relation to future earthquake potential in Kamchatka. In: Seismogenic and Tsunamigenic Processes in Shallow Subduction Zones. Birkhäuser, Basel, pp. 541–553.
Kelsey, H.M., Witter, R.C., Engelhart, S.E., Briggs, R., Nelson, A., Haeussler, P., Corbett, D.R., 2015. Beach ridges as paleoseismic indicators of abrupt coastal subsidence during subduction zone earthquakes, and implications for Alaska-Aleutian subduction zone paleoseismology, southeast coast of the Kenai Peninsula, Alaska. Quat. Sci. Rev. 113, 147–158.
Kobayashi, T., Tobita, M., Nishimura, T., Suzuki, A., Noguchi, Y., Yamanaka, M., 2011. Crustal deformation map for the 2011 off the Pacific coast of Tohoku Earthquake, detected by InSAR analysis combined with GEONET data. Earth Planets Space 63 (7) article 20. https://earth-planets-space.springeropen.com/articles/10.5047/eps.2011.06.043.
Kravchunovskaya, E.A., Myalo, E.G., Pinegina, T.K., Sidneva, E.N., 2010. Vegetation of Holocene marine terraces as a reflection of the history of coastal development (Kamchatka Peninsula). In: Proceedings of the IV Sakhalin Youth Scientific School "Natural Catastrophes: Study, Monitoring, and Forecast. Yuzhno-Sakhalinsk, pp. 286–292 (in Russian).
Kyle, P.R., Ponomareva, V.V., Rourke Schluep, R., 2011. Geochemical characterization of marker tephra layers from major Holocene eruptions, Kamchatka Peninsula, Russia. Int. Geol. Rev. 53 (9), 1059–1097.
Lander, A.V., Shapiro, M.N., 2007. The origin of the modern Kamchatka subduction zone. In: Eichelberger, J., et al. (Eds.), Volcanism and Subduction: the Kamchatka Region, pp. 57–64.
Lay, T., Kanamori, H., Ammon, C.J., Hutko, A.R., Furlong, K., Rivera, L., 2009. The 2006–2007 Kuril Islands great earthquake sequence. J. Geophys. Res.: Solid Earth 114 (B11).
Leonard, L.J., Hyndman, R.D., Mazzotti, S., 2004. Coseismic subsidence in the 1700 great Cascadia earthquake: coastal estimates versus elastic dislocation models. Geol. Soc. Am. Bull. 116 (5–6), 655–670.
Leonard, L.J., Currie, C.A., Mazzotti, S., Hyndman, R.D., 2010. Rupture area and displacement of past Cascadia great earthquakes from coastal coseismic subsidence. Bull. Seismol. Soc. Am. 122 (11–12), 2079–2096.
Lowe, D.J., 2011. Tephrochronology and its application: a review. Quat. Geochronol. 6, 107–153.
MacInnes, B., Bourgeois, J., Pinegina, T.K., Kravchunovskaya, E.A., 2009. Before and after: geomorphic change from the 15 November 2006 Kuril Island tsunami. Geology 37 (11), 995–998.
MacInnes, B.T., Weiss, R., Bourgeois, J., Pinegina, T.K., 2010. Slip distribution of the 1952 Kamchatka great earthquake based on near-field tsunami deposits and historical records. Bull. Seismol. Soc. Am. 100 (4), 1695–1709.
Martin, M.E., Weiss, R., Bourgeois, J., Pinegina, T.K., Houston, H., Titov, V.V., 2008. Combining constraints from tsunami modeling and sedimentology to untangle the 1969 Ozernoi and 1971 Kamchatskii tsunamis. Geophys. Res. Lett. 35 (1), L01610.
McSaveney, M.J., Graham, I., Begg, J., Beau, A., Hull, A., Kim, K., Zondervan, A., 2006. Late Holocene uplift of beach ridges at Turakirae Head, south Wellington coast, New Zealand. N. Z. J. Geol. Geophys. 49, 337e358.
Melnick, D., Cisternas, M., Moreno, M., Norambuena, R., 2012. Estimating coseismic coastal uplift with an intertidal mussel: calibration for the 2010 Maule Chile earthquake (Mw= 8.8). Quat. Sci. Rev. 42, 29–42.
Meltzner, A.J., Sieh, K., Abrams, M., Agnew, D.C., Hudnut, K.W., Avouac, J.P., Natawidjaja, D.H., 2006. Uplift and subsidence associated with the great Aceh–Andaman earthquake of 2004. J. Geophys. Res.: Solid Earth 111 (B2).
Meyers, R.A., Smith, D.G., Jol, H.M., Peterson, C.D., 1996. Evidence for eight great earthquake- subsidence events detected with ground-penetrating radar, Willapa barrier. Wash. Geol. 24 (2), 99–102.
Melnick, D., Bookhagen, B., Echtler, H.P., Strecker, M.R., 2006. Coastal deformation and great subduction earthquakes, Isla Santa María, Chile (37S). Geol. Soc. Am. Bull. 118 (11–12), 1463–1480.
Monecke, K., Templeton, C.K., Finger, W., Houston, B., Luthi, S., McAdoo, B.G., Meilianda, E., Storms, J.E., Walstra, D.J., Amna, R., Hood, N., 2015. Beach ridge patterns in West Aceh, Indonesia, and their response to large earthquakes along the northern Sunda trench. Quat. Sci. Rev. 113, 159–170.
Monecke, K., Meilianda, E., Walstra, D.-J., Hill, E.M., McAdoo, B.G., Qiu, Q., Storms, J.E.A., Masputri, A.S., Mayasari, C.D., Nasir, M., Riandi, I., Setiawan, A., Templeton, C.K., 2017. Postseismic coastal development in Aceh, Indonesia–Field observations and numerical modelling. Mar. Geol. 392, 94–104.
Moreno, M., Melnick, D., Rosenau, M., Baez, J., Klotz, J., Oncken, O., Tassara, A., Chen, J., Bataille, K., Bevis, M., Socquet, A., 2012. Toward understanding tectonic control on the Mw 8.8 2010 Maule Chile earthquake. Earth Planet Sci. Lett. 321, 152–165.
Morton, R.A., Gelfenbaum, G., Buckley, M.L., Richmond, B.M., 2011. Geological effects and implications of the 2010 tsunami along the central coast of Chile. Sediment. Geol. 242 (1–4), 34–51.
Nelson, A.R., Shennan, I., Long, A.J., 1996. Identifying coseismic subsidence in tidal–wetland stratigraphic sequences at the Cascadia subduction zone of western North America. J. Geophys. Res.: Solid Earth 101 (B3), 6115–6135.
Okada, Y., 1985. Surface deformation due to shear and tensile faults in a half-space. Bull. Seismol. Soc. Am. 75 (4), 1135–1154.
Peterson, C.D., Doyle, D.L., Barnett, E.T., 2000. Coastal flooding and beach retreat from coseismic subsidence in the central Cascadia margin, USA. Environ. Eng. Geosci. 6 (3), 255–269.
Peterson, C.D., Jol, H.M., Vanderburgh, S., Phipps, J.B., Percy, D., Gelfenbaum, G., 2010. Dating of late Holocene beach shoreline positions by regional correlation of coseismic retreat events in the Columbia River littoral cell, USA. Mar. Geol. 273 (1–4), 44–61.
Phipps, J., Jol, H.M., Peterson, C.D., Vanderburgh, S., 2001. Sand dune reactivation and subduction zone earthquakes in the Grayland area. Wash. Geol. 28 (3), 31–33.
Pilarczyk, J.E., Dura, T., Horton, B.P., Engelhart, S.E., Kemp, A.C., Sawai, Y., 2014. Microfossils from coastal environments as indicators of paleo-earthquakes, tsunamis and storms. Palaeogeogr. Palaeoclimatol. Palaeoecol. 413, 144–157.
Pinegina, T.K., 2014. Time-space Distribution of Tsunamigenic Earthquakes along the Pacific and Bering Coasts of Kamchatka: Insight from Paleotsunami Deposits. Doctor of Geological Science dissertation, Institute of Oceanology RAS, Moscow, p. 235 (in Russian). http://www.ocean.ru/disser/index.php/dissertatsii/file/62-tekst-dissertatsii-pinegina.html.
Pinegina, T.K., Bourgeois, J., 2020. Tephrostratigraphy and tephrochronology. In: Brill, D., et al. (Eds.), Geological Records of Tsunamis and Other Extreme Waves. Elsevier. In press.
Pinegina, T.K., Bourgeois, J., Kravchunovskaya, E.A., Lander, A.V., Arcos, M.E., Pedoja, K., MacInnes, B.T., 2013. A nexus of plate interaction: vertical deformation of Holocene wave-built terraces on the Kamchatsky Peninsula (Kamchatka, Russia). Bull. Geol. Soc. Am. 125 (9–10), 1554–1568.
Pinegina, T.K., Bazanova, L.I., Zelenin, E.A., Bourgeois, J., Kozhurin, A.I., Medvedev, I.P., Vydrin, D.S., 2018. Holocene tsunamis in Avachinsky bay, Kamchatka, Russia. Pure Appl. Geophys. 175 (4), 1485–1506. https://link.springer.com/article/10.1007/s00024-018-1830-0#SupplementaryMaterial.
Plafker, G., 1965. Tectonic deformation associated with the 1964 Alaska earthquake: the earthquake of 27 March 1964 resulted in observable crustal deformation of unprecedented areal extent. Science 148 (3678), 1675–1687.
Plafker, G., 1969. Tectonics of the March 27, 1964 Alaska earthquake: U.S. Geological Survey Professional Paper 543-I, p. 74, 2 sheets, scales 1:2,000,000 and 1:500,000. https://pubs.usgs.gov/pp/0543i/.
Plafker, G., Savage, J.C., 1970. Mechanism of the Chilean earthquakes of May 21 and 22, 1960. Bull. Geol. Soc. Am. 81 (4), 1001–1030.
Ponomareva, V., Portnyagin, M., Pendea, F., Zelenin, E., Bourgeois, J., Pinegina, T., Kozhurin, A., 2017. A full Holocene tephrochronology for the Kamchatsky Peninsula region: applications from Kamchatka to north America. Quat. Sci. Rev. 168, 101–122.
Richmond, B., Szczuciński, W., Chagué-Goff, C., Goto, K., Sugawara, D., Witter, R., et al., 2012. Erosion, deposition and landscape change on the Sendai coastal

plain, Japan, resulting from the March 11, 2011 Tohoku-oki tsunami. Sediment. Geol. 282, 27–39.
Saltonstall, P., Carver, G.A., 2003. Earthquakes, subsidence, prehistoric site attrition and the archaeological record: a view from the Settlement Point site, Kodiak Archipelago, Alaska. In: Natural Disasters and Cultural Change. Routledge, pp. 188–208.
Satake, K., Wang, K., Atwater, B.F., 2003. Fault slip and seismic moment of the 1700 Cascadia earthquake inferred from Japanese tsunami descriptions. J. Geophys. Res.: Solid Earth 108 (B11).
Satake, K., Nanayama, F., Yamaki, S., 2008. Fault models of unusual tsunami in the 17th century along the Kuril trench. Earth Planets Space 60 (9), 925–935.
Satake, K., 2015. Geological and historical evidence of irregular recurrent earthquakes in Japan. Phil. Trans. Math. Phys. Eng. Sci. 373 (2053), 20140375.
Shennan, I., Hamilton, S., 2006. Coseismic and pre-seismic subsidence associated with great earthquakes in Alaska. Quat. Sci. Rev. 25 (1–2), 1–8.
Sieh, K., Natawidjaja, D.H., Meltzner, A.J., Shen, C.C., Cheng, H., Li, K.S., Suwargadi, B.W., Galetzka, J., Philibosian, B., Edwards, R.L., 2008. Earthquake supercycles inferred from sea-level changes recorded in the corals of west Sumatra. Science 322 (5908), 1674–1678.
Simms, A.R., DeWitt, R., Zurbuchen, J., Vaughan, P., 2017. Coastal erosion and recovery from a Cascadia subduction zone earthquake and tsunami. Mar. Geol. 392, 30–40.
Tamura, T., 2012. Beach ridges and prograded beach deposits as palaeoenvironment records. Earth Sci. Rev. 114 (3–4), 279–297.
Thatcher, W., Rundle, J.B., 1979. A model for the earthquake cycle in underthrust zones. J. Geophys. Res.: Solid Earth 84 (B10), 5540–5556.
Udo, K., Sugawara, D., Tanaka, H., Imai, K., Mano, A., 2012. Impact of the 2011 Tohoku earthquake and tsunami on beach morphology along the northern Sendai coast. Coast Eng. J. 54, 1250009, 01.
Wang, P.-L., Engelhart, S.E., Wang, K., Hawkes, A.D., Horton, B.P., Nelson, A.R., Witter, R.C., 2013. Heterogeneous rupture in the great Cascadia earthquake of 1700 inferred from coastal subsidence estimates. J. Geophys. Res. Solid Earth 118, 2460–2473.
Witter, R.C., Zhang, Y.J., Wang, K., Priest, G.R., Goldfinger, C., Stimely, L., et al., 2013. Simulated tsunami inundation for a range of Cascadia megathrust earthquake scenarios at Bandon, Oregon, USA. Geosphere 9 (6), 1783–1803.